Equilibration of a baroclinic planetary atmosphere toward the limit of vanishing bottom friction

JUNYI CHAI* †

Atmospheric and Oceanic Sciences Program, Princeton University, Princeton, NJ, USA

MALTE JANSEN

Department of the Geophysical Sciences, The University of Chicago, Chicago, IL, USA

GEOFFREY K. VALLIS

Department of Mathematics, University of Exeter, Exeter, UK

* *Corresponding author address:* Junyi Chai, Atmospheric and Oceanic Sciences Program, Princeton University, New Jersey, USA

E-mail: junyic@princeton.edu

†

ABSTRACT

This paper discusses whether and how a baroclinic atmosphere can equilibrate with very small bottom friction in a dry, primitive equation, general circulation model. The model is forced by a Newtonian relaxation of temperature to a prescribed temperature profile, and it is damped by a linear friction near the lower boundary. When friction is decreased by four orders of magnitude, kinetic energy dissipation by friction gradually becomes negligible, while "energy recycling" becomes dominant. In this limit kinetic energy is converted back into potential energy at the largest scales, thus closing the energy cycle without significant frictional dissipation. The momentum fluxes are of opposite sign in the upper and lower atmosphere: in the upper atmosphere, eddies converge momentum into the westerly jets, however, in the lower atmosphere, the eddies diverge momentum out of the westerly jets. The secondary circulation driven by the meridional eddy momentum fluxes thus acts to increase the baroclinicity of the westerly jet. This regime may be relevant for the Jovian atmosphere, where the frictional time scale may be much larger than the radiative damping time scale.

1. Introduction

Bottom friction (also referred to as surface drag) that acts at large scales plays a crucial role in the equilibration of baroclinic turbulence for Earth's atmosphere. The importance of bottom friction can be illustrated by considering the momentum and energy budgets. The zonal-mean angular momentum budget at midlatitudes is characterized by a transfer of angular momentum from the eddies into the westerly jets. In a statistically steady state this momentum-flux convergence must be balanced by frictional drag in the bottom boundary layer (Green 1970; Held 1975; Edmon et al. 1980). The energy budget is constrained by the quasi-two-dimensional character of the large-scale dynamics. Little kinetic energy generated by baroclinic instability can cascade to smaller scales (see a review on two-dimensional turbulence by Boffetta and Ecke 2012); instead, most kinetic energy cascades to larger scales or gets channeled into the zonal jets (Vallis and Maltrud 1993). The bottom drag is needed to ultimately remove the kinetic energy, thus closing the energy cycle and bounding the kinetic energy. By considering the atmosphere to work as a heat engine, the entropy budget provides an additional perspective (Held 2007). The large scale radiative damping decreases the entropy of the flow, as the warmer equatorial region gets heated and polar region gets cooled. In a statistical steady state, the decrease in entropy is balanced by the creation of entropy due to bottom friction for the dry dynamics.

Such budgets are less clear for Jupiter's atmosphere or the atmospheres of other Jovian planets as the strength of bottom friction is highly uncertain. In one line of studies, a model for Jupiter's atmospheric circulation considers a thin shell upper atmosphere (~ 1 bar) sitting on top of a deep fluid interior. The upper atmosphere is often referred as the weather layer for it is hypothesized to be Earth-like: the flow is governed by similar geophysical fluid dynamics as Earth, and the strong jets and turbulent eddies are energized by baroclinic instability or by convection coupled to large scale dynamics, with the deep interior rather crudely treated as a lower boundary condition (Williams and Halloway 1982; Williams 1985; see a review by Vasavada and Showman 2005). In modeling the circulation of the weather layer, a major uncertainty lies in the strength of bottom friction, which parameterizes the coupling between the thin weather layer and the deep interior. As a gas giant planet, Jupiter's atmosphere transits smoothly into its deep fluid interior, while the flow is only visible at the cloud top ($0.5 \sim 1$ bar). To find a rigid bottom boundary on Jupiter that may be analogous to Earth's surface, one needs to reach far down below the weather layer, perhaps up to about 0.8 Jupiter's radius, where the pressure reaches more than 10^6 bar so that the molecular hydrogen transits into metallic hydrogen and can be viewed as in near solid-body rotation (Guillot 2005). On the one hand, bottom friction acting on the weather layer thus must be very small or even vanishing as the weather layer does not have a rigid bottom boundary or topography (Dowling 1995). On the other hand, some coupling between the metallic hydrogen interior and the weather layer is expected, otherwise there is nothing unique about the reference frame rotating with the metallic hydrogen core (the existence of latitudinal jets on Uranus suggests that the jets are controlled by internal rotation [Ingersoll 1990]).

Most researchers have in fact included a bottom friction with a somewhat arbitrary strength when modeling the weather layer (e.g., Williams 1985), although the source of the drag remains unclear. One possibility (Showman et al. 2006; Lian and Showman 2008; Schneider and Liu 2009) is that a mean meridional circulation, akin to the Ferrel cell in Earth's atmosphere, extends from the deep interior to the weather layer. If this were to couple the magnetohydrodynamic (MHD) drag in the interior to the weather layer it could act as a kind of drag and allow the weather layer to equilibrate (Liu and Schneider 2010, 2011), and/or explain how shallow forcing at the cloud level could drive deep jets in the interior (Lian and Showman 2008). Still, there is evidently much uncertainty in the mechanism of bottom friction, and hence the effective drag could be extremely small.

Intuitively it might seem hard for an atmosphere to equilibrate in the limit of vanishing bottom friction. It is well-known that for two-dimensional turbulence driven by random stirring, energy will keep accumulating at the largest scale with time in the absence of large scale friction (Kraichnan 1967; Smith and Yakhot 1993; Chertkov et al. 2007). In a primitive equation model simulating Jupiter's upper atmosphere, Liu and Schneider (2015) varied the frictional drag time scale by 3 orders of magnitude and found that the energy dissipation rate, which scales with U^2/τ_f, stays nearly constant (U is a scale for zonal wind speed and τ_f is the frictional damping time scale). In their simulation, the fixed surface heating induces convective stirring at the grid scale, which generates most of the kinetic energy and is similar to the random stirring in two-dimensional turbulence studies. However, for a flow self-stirred by baroclinic instability, the behavior is expected to be different as the stirring itself is influenced by the large scale flow. Interestingly, Lian and Showman (2008) simulated multiple jets driven by baroclinic instability in a primitive equation model with *zero* bottom friction. Although not explicitly studied, it appears that the flow approaches equilibrium after thousands of days of integration (see their Fig. 5).

It is not known whether a high or low value of friction produces more realistic Jovian atmospheric simulations. More fundamentally, the question of whether a baroclinic atmosphere can equilibrate as surface friction tends to zero remains open. In this study we therefore focus on the effects of bottom friction, and in particular the behaviour of a baroclinic atmosphere in both Earth-like and Jovian regimes, as friction becomes very small. Understanding the pathways between the production and dissipation of energy are central to our understanding of baroclinic turbulence in this limit, and three hypotheses concerning the kinetic energy production rate ε suggest themselves.

1. The energy production rate ε stays finite, while the total kinetic energy increases without bound to maintain the necessary frictional dissipation, as in two-dimensional turbulence. This limit is implied by Held and Larichev's (1996) scaling that in a two layer quasi-geostrophic model, the kinetic energy production rate scales as $\varepsilon \sim U^5/(\beta^2 L_R^5)$, where U is the mean thermal wind, β is the planetary vorticity gradient, and L_R is the Rossby deformation radius. In the pure form of this scaling, ε does not depend on bottom friction, which agrees with Liu and Schneider's (2015) simulation. To be a physically realizable system, some mechanism must eventually bound the energy level when the friction becomes small enough. For example, at some point the Rossby number may become sufficiently large so that the flow is no longer quasi two-dimensional and thus allows a forward cascade, in which case ε can be balanced by dissipation at small scales.

2. The energy production rate ε approaches zero as the flow becomes stabilized by the barotropic flow, and the flow ends up in a zonally symmetric state. James and Gray (1986) found that when bottom friction is reduced, the baroclinic instability of the time mean flow is greatly suppressed. This is explained by the increase of the barotropic shear when friction is reduced, which reduces the growth rate of the most unstable mode. It is coined as the "barotropic governor" mechanism (James and Gray 1986; James 1987). It is conceivable that toward the zero friction limit, the "barotropic governor" may become so strong that it completely suppresses the baroclinic instability. This could happen either with the barotropic flow equilibrating at a finite value or there could be a singular limit, in which the kinetic energy diverges but the divergence is such that the energy dissipation rate still goes to zero. The thermal mean state in this case would have to be such that the radiative forcing no longer represents an entropy sink (since there is no obvious source of entropy).

3. The total energy generation and dissipation rate goes to zero, but the flow remains turbulent with a significant energy cycle. This could happen in the following way. At the Rossby deformation radius, eddies convert available potential energy (APE) into eddy kinetic energy (EKE). The EKE then cascades to larger scales, but instead of being accumulated at the largest scale, the inverse cascade is halted at some scale where kinetic energy is converted back into APE, and APE is ultimately dissipated by long wave radiation. For the whole flow, the net ε is negligible: radiative forcing would not generate or dissipate APE. In terms of entropy, radiative forcing would again not be a significant sink of entropy. This mechanism is essentially conjectured by Showman (2007) for Jupiter's atmosphere to equilibrate with little friction. In a shallow water system, it is well-known that the flow can equilibrate without friction, but solely damping of the height perturbation, which represents radiative damping (Showman and Ingersoll 1998; Showman 2007; Scott and Dritschel 2013). However, it is not clear whether this mechanism can work in a continuously stratified flow which possesses a barotropic mode.

To see which is a physically realizable limit, we use an idealized, dry, primitive equation model to simulate a baroclinic atmosphere with varying bottom friction. The model setup and experiments are discussed in Section 2. The simulation results and analysis are discussed in Section 3, The results suggest that a mixture between the second and third hypothesis above is most applicable. The implications of our results and their relevance for Jupiter's atmosphere are discussed in Section 4.

2. Idealized GCM and experiments

We investigate whether and how a baroclinic atmosphere can equilibrate close to the limit of vanishing bottom friction in an idealized GCM, which is set to either Earth-like or Jupiter-like parameters. The general model description is given in subsection a, and the settings that are specific for Earth or Jupiter are described in subsection b and c respectively.

a. Model description

The GCM consists of the Geophysical Fluid Dynamical Laboratory (GFDL) spectral atmospheric dynamical core with the Held and Suarez (1994) forcing, which is a thermal relaxation back to a specified temperature. The model solves the primitive equations for a dry ideal gas atmosphere on a sphere in $\sigma-$coordinate with the spectral transform method in the horizontal, and centered difference scheme in the vertical. There is no bottom topography at the lower boundary. The bottom friction is represented by a Rayleigh damping of horizontal velocities near the lower boundary,

$$\frac{\partial \mathbf{v}}{\partial t} = ... - k(\sigma)\mathbf{v}, \tag{1}$$

where the drag coefficient $k(\sigma)$ decreases linearly from its maximum value k_f at the bottom boundary ($\sigma = 1$) to zero at $\sigma_b = 0.7$,

$$k(\sigma) = k_f \max(0, \frac{\sigma - \sigma_b}{1 - \sigma_b}). \tag{2}$$

Radiative effects are represented by a Newtonian relaxation of temperature to a prescribed "radiative-convective equilibrium" profile,

$$\frac{\partial T}{\partial t} = ... - \alpha_T(T - T_{eq}), \tag{3}$$

where the forcing rate α_T adopts the same value everywhere ($\alpha_T = 1/40$ day^{-1}, Earth day is used thereinafter). The prescribed profile T_{eq} is zonally symmetric, and it is chosen to be suitable for either Earth or Jupiter (see subsections below). Apart from the Rayleigh friction and Newtonian heating, the only other dissipative process is an 8th order hyper-diffusion ∇^8 imposed on vorticity, divergence and temperature fields, with a damping time scale of 0.1 day for the smallest waves.

The initial condition is an isothermal state (200 K) at rest in the rotating reference frame, with some small temperature perturbation to break the zonal symmetry. If the bottom friction is identically zero, the climatology will inevitably depend on the initial condition, as the total angular momentum must be conserved if there is no friction. We will thus restrict our simulations to the limit of very small but finite friction, and return to a discussion of the zero friction limit at the end.

b. Earth-like simulations

In this subsection we discuss simulations using Earth parameters, i.e., Earth's radius, rotation rate, and the gas constant of air. The "equilibrium" temperature profile T_{eq} is adapted from Held and Suarez (1994) as

$$T_{eq} = \max\left\{T_{st}, \left[T_0 - \Delta_y T \sin^2\phi - \Delta_z\theta \ln\left(\frac{p}{p_0}\right)\right]\left(\frac{p}{p_0}\right)^{\kappa}\right\}, \tag{4}$$

where $T_{st} = 200\,\mathrm{K}$ is the stratospheric equilibrium temperature, $T_0 = 315\,\mathrm{K}$ is the equatorial equilibrium temperature at the surface, $\Delta_y T = 60\,\mathrm{K}$ sets the meridional temperature gradient, and $\Delta_z\theta$ sets the vertical static stability. The reference pressure $p_0 = 1000$ mb and $\kappa = 2/7$. The only difference with the original Held and Suarez's (1994) profile is that we relax to a stable static stability profile everywhere in the troposphere, while Held and Suarez (1994) only apply it within the tropics. This prescribed vertical stability may be interpreted as a crude parameterization of unresolved moist convective processes. From a modeling perspective, our main concern is to limit gravitational instability and the associated grid-scale convection (Frierson et al. 2007), which are not properly simulated by our hydrostatic GCM and are resolution dependent. We aim to only simulate the large scale motions related to baroclinic instability, i.e., baroclinic turbulence. The vertical stability parameter is chosen as $\Delta_z\theta = 20\,\mathrm{K}$. As the criticality $\xi \sim \Delta_y T/\Delta_z\theta$ for the equilibrium temperature profile is larger than 1, the eddies will tend to increase vertical stability so as to reduce criticality to ∼1 (Schneider and Walker 2006; Chai and Vallis 2014; Jansen and Ferrari 2013). Therefore, the lower limit for the Rossby radius can be estimated from the equilibrium temperature profile as $L_R \sim \sqrt{R\Delta_z\theta}/f$.[1] Choosing the midlatitude value for the Coriolis parameter as $f \sim 10^{-4}$ s^{-1}, the lower limit for the Rossby radius is about $L_R \sim 760$ km or spherical wavenumber ∼26.

Bottom friction is reduced towards the zero limit by varying the frictional damping time scale $\tau_f = 1/k_f$ across 4 orders of magnitude: $\tau_f = 1$ (control), 10, 10^2, 10^3, and 10^4 days. The largest frictional value $\tau_f = 1$ day is used by Held and Suarez (1994) to produce an Earth-like climate. We use T42 resolution in the horizontal and 30 evenly spaced σ levels in the vertical. This choice sacrifices resolution in the stratosphere but allows for better resolution of the baroclinic eddies in the troposphere as in the previous studies (Held and Larichev 1996; Zurita-Gotor 2008; Chen and Plumb 2014; Lorenz 2015). All simulations are integrated for 30,000 days, except that the lowest friction simulation ($\tau_f = 10^4$ day) is integrated for 60,000 days to reach a statistically steady state. At T42 resolution, the Rossby radius should be adequately resolved. In order to study the dynamical convergence of the flow field with horizontal resolution, we repeat the simulations using T127 resolution. For the simulation with $\tau_f = 10^3$ days, one additional run using T213 resolution is further carried out.

c. Jupiter-like simulations

Similar to the Earth-like simulations, the Jupiter model simulates a thin shell atmosphere extending from the top of the atmosphere to an artificial rigid lower surface. The mean surface pressure

---

[1]The Rossby radius is usually estimated as $L_R = N_p(p_s - p_t)/f$, where $N_p^2 = -(\rho^s\theta^s)^{-1}\partial_p\theta^s$ is a vertical stability measure; p_s and p_t are the surface pressure and tropopause pressures respectively; θ is potential temperature and the superscript s denotes that the value is taken near the surface (Merlis and Schneider 2009; Chai and Vallis 2014). Approximations are made such that $p_s - p_t \sim p_s$, $(p_s - p_t)\partial_p\theta^s \sim \Delta_z\theta$, $\rho^s\theta^s = \rho^s T^s(p_0/p_s)^\kappa \sim \rho^s T^s = p_s/R$, therefore we obtain $L_R \sim \sqrt{R\Delta_z\theta}/f$.

is 3 bar, which is used in a series of studies by Schneider and Liu (Schneider and Liu 2009; Liu and Schneider 2010, 2011, 2015). The planetary parameters are set to those of Jupiter: planetary radius $a = 6.986 \times 10^4$ km, planetary angular velocity $\Omega = 1.7587 \times 10^{-4}$ s^{-1}, and specific gas constant $R = 3605.38$ J kg^{-1}K^{-1}(Liu and Schneider 2010). The equilibrium temperature profile roughly represents Jupiter, and is similar to that used by Lian and Showman (2008):

$$T_{eq} = T_{ref}(p) + \delta T(\phi). \tag{5}$$

In the vertical direction, the reference temperature profile T_{ref} corresponds to an isothermal stratosphere at 110 K above 0.15 bar level, a troposphere with some vertical stability specified by $\Delta_z \theta$, and a smooth transition between them. Analytically, it is

$$T_{ref}(p) = G(p)T_{st} + [1 - G(p)]\,[T_0 - \Delta_z \theta \ln(p/p_0)]\,(p/p_0)^{\kappa}, \tag{6}$$

where the stratosphere temperature $T_{st} = 110$ K, the reference pressure $p_0 = 1000$ mb, the temperature at reference pressure $T_0 = 170$ K, and $\kappa = 2/7$. $G(p) = [1 - (p/p_{trop})^2]^{-1}$ marks the transition from the stratosphere to the troposphere at $p_{trop} = 150$ mb. The vertical stability is $\Delta_z \theta = 5$ K. Therefore, the lower limit for the Rossby radius is about 1000 km at midlatitudes, or a spherical wavenumber of about 200. In the meridional direction, a temperature gradient is imposed to drive baroclinic turbulence

$$\delta T(\phi) = \Delta_y T \left[1/3 - \sin^2(\phi)\right], \tag{7}$$

where the equator-pole temperature difference is set to $\Delta_y T = 15$ K. This value is significantly larger than the latitudinal temperature difference observed in Jupiter's upper atmosphere (0$\sim$0.5 bar), which is typically around 5 K (Simon-Miller et al. 2006), although it is comparable to Schneider and Liu's (Schneider and Liu 2009; Liu and Schneider 2010, 2011, 2015) series of Jupiter simulations, where the equator-pole temperature difference in equilibrium is about 12 K. From a modeling perspective, using a smaller $\Delta_y T$ (we have tested 10 K) results in weaker baroclinic eddy activity as the criticality $\xi \sim \Delta_y T/\Delta_z \theta$ becomes small, although strong jets can form with quite weak baroclinicity (Kaspi and Flierl 2007). Reducing vertical stability $\Delta_z \theta$ can maintain the same criticality and thus keep strong eddy activity even for smaller $\Delta_y T$. However, smaller vertical stability leads to smaller Rossby radius and therefore requires higher resolution.

We consider five different values of bottom friction: $\tau_f = 5$, 50, 500, and 5000 days. The simulations are integrated for 20,000 days at T213 resolution. There are 30 unevenly spaced σ levels, chosen such that there are equal number of levels in the stratosphere and troposphere. All simulations are initialized from an isothermal motionless atmosphere with small thermal perturbations, except for the $\tau_f = 5000$ day run, which is initialized from the end of the $\tau_f = 50$ day run and yields better hemispheric symmetry (the low friction simulations are dependent on initial condition due to jet merging during model spin-up).

3. Results

Although our motivation arises, at least in part, from Jupiter's atmosphere, most of our conclusions are universal for a dry baroclinic atmosphere and apply in both Jovian and Earth-like regimes. The Earth-like simulations are more efficient to run and diagnose, and we will thus mostly show results from the Earth-like simulations, and resort to Jupiter-like simulations when they provide additional insights. If not specified, the simulations refer to the Earth-like simulations.

a. Basic climatology

To see whether the atmosphere has equilibrated, we calculate the time evolution of the global averaged kinetic energy (KE) and eddy kinetic energy (EKE) per unit mass (with unit $\mathrm{m^2 s^{-2}}$), as shown in Fig. 1. For simulations with $\tau_f = 1$ to 10^3 days, the flow equilibrates after a few hundred to a few thousand days. For the $\tau_f = 10^4$ days run, the flow is initially close to a zonally symmetric state as the EKE is negligible. Until at about 23,000 days, the flow abruptly transits into an eddying state and then equilibrates with large fluctuations. For $\tau_f = 10^3$ and 10^4 days runs, there is long term variability on the time scale of hundreds to thousands of days, but on an even longer time scale, the flow appears to be equilibrated. The long term variability for low friction runs is also seen in James and Gray's (1986) simulations. In their lowest friction simulation, the flow is nearly zonally symmetric similar to our run with $\tau_f = 10^4$ days in the first 10,000 days. However, they did not observe the regime transition into a strongly eddying state possibly because their simulations are limited to 500 days. When the bottom friction is reduced from $\tau_f = 1$ to 10^4 days, the average KE increases monotonically. However, the average EKE is not monotonic with friction. Instead, the average EKE decreases when friction is reduced from $\tau_f = 1$ to 10^2 days and then increases when friction is further reduced.

Fig. 2 shows the climatology for the series of runs with different surface friction. The control run with $\tau_f = 1$ day is comparable to Earth's climate. When friction is reduced, the jets become stronger and sharper, and become dominated by their barotropic components. Near the surface, the eddy potential temperature (PT) flux moves equatorward from the midlatitudes. Comparison to the Jupiter-like simulations shown in Fig. 3 suggests that more generally the eddy PT flux moves from the westerly jet regions into the easterly jet regions when surface friction is reduced. This may be understood from the fact that a sharp westerly jet is known to suppress mixing across it (Dritschel and McIntyre 2008). In Earth's atmosphere, the jet-stream near the tropopause forms a north-south mixing barrier (Mahlman 1997). In our simulations when surface friction is low enough, the jet-stream extends all the way to the surface, thus suppressing mixing even near the surface. Therefore, the baroclinic eddy activity moves into the easterly jets in the presence of sharp barotropic westerly jets. Notice that when friction is small, there is significant latitudinal surface pressure variation, which is required to support strong barotropic jets. This causes some missing contours near 1000 mb in Fig. 2 and near 3000 mb in Fig. 3, as there is no flow field at the given pressure level and latitude. In Fig. 3, the lack of super-rotation at the equator in our Jupiter-like simulations compared with Schneider and Liu (2009) might be due to the lack of internal heating and therefore a lack of strong convective instability at the equator. We specifically want to suppress this energy source in order to focus on baroclinic turbulence only.

To get an impression on the characteristics of the flow, snapshots of instantaneous fields are shown in Figs. 4 and 5. Ertel's potential vorticity (PV) on isentropic surface $\theta = 330$ K, calculated as

$$PV = -g(\zeta + f)\frac{\partial \theta}{\partial p}, \tag{8}$$

is shown in Fig. 4 for Earth-like simulations with high (τ_f =1 day) and low ($\tau_f = 10^3$ and 10^4 days) surface friction (Haynes and McIntyre 1987). For all simulations, Ertel's PV has a sharp gradient across the jet stream. In the simulation with τ_f= 1 day, the jet meanders strongly and filaments indicate wave-breaking and mixing of PV. In $\tau = 10^3$ and 10^4 days simulations, the jet stream is more regular and is visually similar to the stratospheric vortex. Wave breaking is hardly seen. For the Jupiter-like simulations, zonal wind fields in the extratropics are shown in Fig. 5. When friction is reduced from $\tau_f = 5$ days to 5000 days, the outer jet seems to get stabilized while eddy activity is confined to latitudes above 45°.

b. Energy cycle

The energy cycle is key to understanding how the model equilibrates close to the limit of vanishing bottom friction. As a reference, the observed Lorenz energy cycle for Earth's atmosphere is shown in Fig. 6a (adapted from Peixto and Oort 1984). In Lorentz's (1955) formalism, the energy is partitioned into available potential energy (APE) and kinetic energy (KE). Furthermore, APE and KE are partitioned into the zonal mean and eddy parts. Differential heating by solar radiation leads to a zonally symmetric temperature distribution with strong meridional temperature gradient at mid-latitudes, thus maintaining the APE of the zonal mean flow (ZAPE). The temperature field is stirred by the eddies which create temperature variance in the zonal direction and thus transferring ZAPE into eddy APE (EAPE, at a rate 1.27 W m^{-2}). Through baroclinic instability, EAPE is next converted into EKE (2.0 W m^{-2}). Some of the EKE is channeled into the zonal mean KE (ZKE) as the eddy momentum flux is up gradient of zonal mean angular velocity and thus accelerates the zonal jets (0.33 W m^{-2}). A majority of EKE is directly dissipated by bottom friction or molecular viscosity (1.7 W m^{-2}). Finally, some of the ZKE is dissipated by bottom friction or viscosity (0.2 W m^{-2}), while a comparable amount is converted into ZAPE (0.15 W m^{-2}). The latter conversion is achieved by the combined effect of the direct and indirect mean meridional circulations: the Hadley cell (direct circulation) generates ZKE, however, the Ferrel cell (indirect circulation) converts ZKE back into ZAPE at a rate exceeding the production rate of the Hadley cell. Therefore, the net conversion is from ZKE into ZAPE[2].

Here we focus on the three energy reservoirs potential energy PE, EKE and ZKE, and we do not explicitly consider the budgets for ZAPE and EAPE since they may not be well defined if the isentropic slope becomes large, as is the case in our simulations with weak friction. In this perspective, the energy cycle for the Earth-like simulation with the largest bottom friction $\tau_f = 1$ day is shown in Fig. 6b and is comparable to the observed energy cycle described above. For our Earth-like simulations with different strength of friction, the energy budgets for EKE, ZKE and

[2]An updated Lorenz energy cycle calculation by Li et al. (2007) using reanalysis datasets shows that near surface processes in the Southern hemisphere play an important role in converting ZAPE into ZKE, and probably change the direction of net conversion rate between ZAPE and ZKE as shown by Peixto and Oort (1984). However, away from the surface, Li et. al. (2007) still supports Peixoto and Oort's (1984) results that the indirect Ferrel cell converts more ZKE into ZAPE than the ZKE produced by the direct Hadley cell, and the net conversion is thus from ZKE to ZAPE.

KE are shown in Fig. 7. The balance equations for EKE and ZKE are

$$\frac{\partial \text{EKE}}{\partial t} = C(\text{PE},\text{EKE}) - C(\text{EKE},\text{ZKE}) - D(\text{EKE}), \tag{9}$$

$$\frac{\partial \text{ZKE}}{\partial t} = C(\text{EKE},\text{ZKE}) - C(\text{ZKE},\text{PE}) - D(\text{ZKE}), \tag{10}$$

where EKE is dissipated by both bottom friction and hyperviscosity as

$$D(\text{EKE}) = D_{fri}(\text{EKE}) + D_{vis}(\text{EKE}), \tag{11}$$

while the hyperviscosity for ZKE is negligible, and therefore

$$D(\text{ZKE}) \simeq D_{fri}(\text{ZKE}). \tag{12}$$

Adding together Eqs. (9) and (10) gives the energy budget for the total flow as

$$\frac{\partial \text{KE}}{\partial t} = C(\text{PE},\text{KE}) - D_{fri}(\text{KE}) - D_{vis}(\text{KE}). \tag{13}$$

The detailed formulations for each term are included in Appendix A. In a statistical steady state, the left hand sides of Eqs. (9), (10) and (13) averaged over time are zero.

We first consider the EKE budget. For the control run ($\tau_f = 1$ day), the EKE generation rate $C(\text{PE},\text{EKE})$ is similar to that observed in Earth's atmosphere. However, contrary to Earth's atmosphere, EKE conversion into ZKE $C(\text{EKE},\text{ZKE})$ is slightly larger than dissipation rate $D(\text{EKE})$. This may be due to the fact that our model only simulates large-scale quasi- two-dimensional motions and does not resolve convection and three dimensional turbulence which can dissipate energy by molecular viscosity. EKE is dissipated mainly by bottom friction, whose dissipation rate is roughly 1 order of magnitude larger than that of hyperviscosity. When bottom friction decreases from $\tau_f = 1$ to 10^3 days, the EKE generation rate $C(\text{PE},\text{EKE})$ decreases monotonically by roughly 1 order of magnitude. This resembles the barotropic governor effect, that strong barotropic jets limit the growth of baroclinic instability. When bottom friction further decreases to $\tau_f = 10^4$ days, the barotropic governor effect appears to saturate, and the EKE generation rate increases slightly. The barotropic governor thus does not appear to be able to totally suppress baroclinic instability. For the whole range of decreasing bottom friction, EKE dissipation by bottom friction decreases monotonically by roughly 3 orders of magnitude. Dissipation by hyperviscosity decreases less than 1 order of magnitude, but is never a dominant term in the EKE budget. In the low friction end, the dominant balance for the EKE budget is between EKE generation $C(\mathrm{PE},\mathrm{EKE})$ and EKE conversion into ZKE $C(\mathrm{EKE},\mathrm{ZKE})$.

Next we will consider the ZKE budget. For the control run ($\tau_f = 1$ day), conversion from EKE into ZKE $C(\mathrm{EKE},\mathrm{ZKE})$ is balanced by frictional dissipation $D_{fri}(\mathrm{ZKE})$ and conversion into PE $C(\mathrm{ZKE},\mathrm{PE})$, which are of similar magnitudes. For τ_f between 10 and 10^2 days, all conversion terms decrease with decreasing friction. When bottom friction further decreases ($\tau_f = 10^3$ and 10^4 days), $C(\mathrm{ZKE},\mathrm{PE})$ saturates, while $D_{fri}(\mathrm{ZKE})$ continues to decrease. In the low friction limit ($\tau_f = 10^4$ days), $D_{fri}(\mathrm{ZKE})$ is negligible compared with $C(\mathrm{ZKE},\mathrm{PE})$, and the primary balance is between $C(\mathrm{EKE},\mathrm{ZKE})$ and $C(\mathrm{ZKE},\mathrm{PE})$. As the energy dissipation by bottom friction is negligible for our lowest friction run ($\tau_f = 10^4$ days), and the effect of hyperviscosity does not strongly influence the large scale motions, the simulation with $\tau_f = 10^4$ days may be regarded as effectively approaching the limit of vanishing bottom friction. In this limit, schematically the dominant energy cycle proceeds from PE and ends at PE:

$$\mathrm{PE} \rightarrow \mathrm{EKE} \rightarrow \mathrm{ZKE} \rightarrow \mathrm{PE}. \tag{14}$$

This energy cycle is illustrated in Fig. 6c. From the structure of PT flux shown in Fig. 2 and 3, we can see that baroclinicity is reduced within the easterly jets. As the net PE conversion into KE is negligible from the above energy cycle, a reduction of baroclinicity in the easterly jets must be balanced by an increase of baroclinicity in the westerly jets, which is achieved by the Ferrel cell. In other words, the effect of eddies and the zonal mean circulation is primarily to redistribute baroclinicity into a latitudinal structure different from that set by differential radiation: the baroclinicity is reduced in the easterly jets and enhanced in the westerly jets. The effect of eddies to enhance the baroclinicity of westerly jets has been seen in the wintertime Earth atmosphere and in numerical models, and is usually referred as self-maintenance of midlatitude jets (Robinson 2006). The mechanism for the self-maintenance of midlatitude jets is shown to be a complicated feedback between waves and the mean flow, but in our low drag simulation, it is required by the structure of PT flux and, most fundamentally, by the energy cycle.

The mean meridional circulation that facilitates the conversion of ZKE into PE is shown in Fig. 8, for simulations with different strength of friction. Here the circulation is averaged over the last 10^4 days of the simulations, and the circulation's structure is quite robust even if a much shorter averaging period is used. When friction reduces from $\tau_f = 1$ to 10^4 days, the meridional circulation develops a complex vertical structure. Still, we can identify a Hadley cell and a Ferrel cell in each hemisphere. The strength of the circulation decreases by roughly about 2 times, which is on the same order as the nearly 3 times decrease in the conversion of ZKE to PE.

For the total flow, the energy budget has a simpler picture as the recycling of kinetic energy at the largest scales are hidden away (Fig. 7 bottom). The the total conversion of PE to KE (which has to approximately equal the generation of PE by the restoring) is balanced by the sum of frictional and viscous dissipation. Dissipation by bottom friction dominates the total energy sink for moderate drag rates, while viscous dissipation starts to dominate the total energy sink in the limit of very small bottom friction. However, this does not mean that the viscous dissipation must have a stronger influence on the synoptic-scale flow as will be discussed in Subsection d. The generation and dissipation rates for total kinetic energy decrease monotonically as friction is reduced. Moreover, in the limit of small friction, the total energy generation and dissipation rates are much smaller than the conversion rates in the ZKE and EKE budgets – indicating the dominant role of energy “recycling”.

A more detailed picture of the energy cycle is provided by the spectral kinetic energy budget. For a compressible fluid, the spectral budget is usually formulated in pressure coordinates in which the KE is a quadratic function of velocity $1/(2g)\int \mathbf{u}^2 dp$ so that KE can be exactly decomposed into each wave vector as $\mathrm{KE}(\mathbf{n}) = 1/(2g)\int \tilde{\mathbf{u}}(\mathbf{n})\cdot\tilde{\mathbf{u}}^*(\mathbf{n})dp$, where $\tilde{\mathbf{u}}(\mathbf{n})$ denotes the spectral coefficient of velocity at wave vector $\mathbf{n}$, and $*$ denotes the complex conjugate (Lambert 1984; Koshyk and Hamilton 2001). In general, the KE is a cubic quantity $1/2\int \rho\mathbf{u}^2 dV$ and thus in other vertical coordinates the KE spectrum is a complicated sum over triads of wave vectors. In this case, density is usually approximated as a constant in order to make KE a quadratic quantity (Waite and Snyder 2009). For Earth’s atmosphere, the pressure coordinate is convenient because a constant 1 bar pressure level is approximately the planetary surface. However in our simulations with low bottom friction, there is large surface pressure variation in the meridional direction in order to support the very strong jets (see Fig. 2, the surface pressure at the poles is significantly lower than 1 bar). Therefore, the usual formalism for the spectral energy budget is not suitable for our purpose, and we derive a new formalism in σ coordinates that gives the approximate spectral KE budget (see Appendix B). For each wavenumber, we can write the spectral KE budget as

$$\partial_t \mathrm{KE}_n \approx G_{KE} + T_{NL} - D_{fri} - D_{vis}, \tag{15}$$

where KE_n denotes the vertically and surface area averaged global KE at total wavenumber n (with unit m^2 s^{-2}); G_{KE} denotes the conversion from potential to kinetic energy; T_{NL} denotes nonlinear kinetic energy transfer from all other wavenumbers into wavenumber n; D_{fri} and D_{vis} denote dissipation by Rayleigh friction and by hyperviscosity respectively.

Similarly, for each wavenumber, the spectral EKE budget is

$$\partial_t \mathrm{EKE}_n \approx G_{EKE} + T_{EE} + T_{EM} - D_{fri} - D_{vis}. \tag{16}$$

Compared with the spectral KE budget, the main difference is that the nonlinear kinetic energy transfer term T_{NL} is further decomposed into T_{EE}, which denotes nonlinear eddy-eddy transfer, and T_{EM}, which denotes the eddy/mean-flow transfer. The difference between KE_n and EKE_n is that EKE_n does not include the spectral components with zonal wavenumber $m = 0$. In a statistically steady state, the left hand sides of Eqs. (15) and (16) averaged over time are zero, which means a balance between the various energy generation, transfer and dissipation terms.

The spectral EKE budget for Earth-like simulations with different bottom frictions are shown in the left panel of Fig. 9. The control run ($\tau_f = 1$ day) resembles Earth's atmosphere: EKE generation peaks at about wavenumber 10; nonlinear eddy-eddy interactions transfer some energy upscale; most energy is transferred into the zonal mean flow or dissipated by bottom friction at scales slightly larger than the EKE generation scale. When friction is reduced to $\tau_f = 10^2$ days, the eddy-eddy interaction and dissipation by bottom friction become negligible, while eddy/mean-flow interactions directly transfer almost all the kinetic energy generated by baroclinic instability into the zonal mean flow at the scale where it is generated. This may be due to the sharpening of the jets, which shear the eddies apart and thus facilitate the energy transfer from eddies into zonal mean flow. When friction further reduces to $\tau_f = 10^4$ days, the spectral budget becomes more jagged. Nevertheless, the eddies are still generating EKE, which is subsequently transferred into the zonal mean flow.

The full spectral KE budget includes the contributions from the zonal mean flow (right panel of Fig. 7). For the control run ($\tau_f = 1$ day), bottom friction dissipates energy across broad scales (wavenumber 3 to 15). KE is generated at wavenumber larger than 4, while KE generation becomes negative at wavenumber 3, which means that KE is converted into PE. As the eddies are generating EKE across all scales as seen from the left panel, the conversion of KE into PE is achieved by the zonal mean flow. Wavenumber 3 corresponds to the zonal jet structure consisting of one easterly jet at the equator and one westerly jet in each hemisphere. Therefore, the conversion of KE back to PE at wavenumber 3 corresponds to the net effect of the Hadley and Ferrel cells as discussed before. When friction is reduced to $\tau_f = 10^2$ days, KE is dissipated by bottom friction almost exclusively in zonal jets with wavenumber 3, where the energy balance is nearly between the up-scale nonlinear transfer and frictional dissipation. Combined with the spectral EKE budget, it means that in physical space, the eddies are generating EKE and transferring EKE into the zonal jets, while bottom friction removes KE only from the zonal jets. When friction further reduces to $\tau_f = 10^4$ days, energy dissipation by bottom friction becomes negligible even for the zonal jets. At wavenumber 3, the major balance is between upscale nonlinear energy transfer and conversion from KE into PE. Combined with the spectral EKE budget, we conclude that in the limit of negligible friction, the energy cycle starts from EKE generation by the eddies, followed by an EKE transfer into the largest zonal jets, and the energy cycle is closed by a conversion of ZKE back into PE by the zonal mean flow.

The spectral EKE budget of the Jupiter-like simulations shows some additional information. As the planetary size is much larger than the deformation radius, there is a clear scale separation between the EKE generating scale and the EKE dissipation scale (or eddy scale), and significant upscale energy transfer by eddy-eddy interactions between the two scales (Fig. 10 top). When friction reduces from $\tau_f = 5$ to 5000 days, the eddy-eddy energy cascade extends to larger scales. The eddy-mean energy transfer becomes positive at the largest scales, which may be a result of barotropic instability associated with the jets and we will return to this below in the discussion of momentum budget. Most importantly, the EKE generation becomes negative at the largest scales, meaning a conversion of EKE into PE. Therefore, the conversion from KE to PE does not have to occur within the zonal mean circulation, but can also occur within the largest eddies. For both Earth-like and Jupiter-like simulations, we do not see a significant change of downscale energy transfer when friction reduces towards zero.

In a shallow water model, the key for KE to convert back into PE is that the horizontal scale of the flow gets larger than the Rossby deformation radius $\sqrt{gH}/f$, where H is the mean layer depth (Scott and Dritschel 2013; Polvani et al. 1994). We suspect that there is also a threshold in the primitive equation model, beyond which the flow can convert KE into PE. In the Earth-like simulations, the domain size is rather limited so that only the scale of the zonal mean flow may be large enough to convert ZKE into PE. Whereas in the Jupiter-like simulations, the much larger domain size permits large enough eddies, which are able to directly convert EKE into PE. Alternatively, the wavy jets in Jupiter-like simulations may project onto the eddy component, without necessarily implying fundamentally different dynamics. This may explain why only in Jupiter-like simulations we observe the conversion of EKE into PE.

To summarize, close to the vanishing friction limit, at small scales eddies convert PE to EKE similar as in Earth's atmosphere. EKE inversely cascades to larger scales and eventually gets channeled into the zonal jets. At the largest scales, the zonal flow and possibly the eddies together convert KE back into PE, thus closing the energy cycle.

c. Momentum budget

In Earth's atmosphere, the Ferrel cell transfers the eddy momentum flux convergence from the upper atmosphere down to the surface where it is balanced by friction (Vallis 2006). In the limit where the surface friction becomes negligible, there is still a Ferrel cell (Fig. 8), whose existence is important for closing the energy cycle. To examine how the momentum is balanced in the vanishing friction limit, we start by reviewing the momentum budget for Earth's atmosphere.

The zonally averaged zonal momentum equation is

$$\frac{\partial \bar{u}}{\partial t} = \bar{v}\left(f - \frac{\partial \bar{u}\cos\phi}{a\cos\phi\partial\phi}\right) - \bar{\omega}\frac{\partial \bar{u}}{\partial p} - \frac{1}{a\cos^2\phi}\frac{\partial\overline{u'v'}\cos^2\phi}{\partial\phi} - \frac{\partial\overline{u'\omega'}}{\partial p} - \bar{F_x}, \tag{17}$$

where a is the planetary radius, $\omega = dp/dt$, ϕ is the latitude, and F_x describes the frictional processes. The overbar denotes a zonal average. In the extratropics, where the Rossby number is small, the time averaged momentum balance for a statistically steady flow is approximately

$$f[\bar{v}] - \frac{1}{a\cos^2\phi}\frac{\partial[\overline{u'v'}]\cos^2\phi}{\partial\phi} - [\bar{F_x}] \approx 0, \tag{18}$$

where the brackets denote a time average (Vallis 2006). In the upper atmosphere, friction is negligible while the eddy momentum flux attains its maximum. Therefore, the balance is between the Coriolis term and eddy momentum flux convergence as

$$f[\bar{v}] \approx \frac{1}{a\cos^2\phi}\frac{\partial[\overline{u'v'}]\cos^2\phi}{\partial\phi}. \tag{19}$$

By mass continuity, a return flow is necessary in the lower atmosphere, and for Earth's atmosphere it occurs within the planetary boundary layer, where friction becomes significant while the wind velocity is relatively small. The dominant momentum balance is thus between the Coriolis term of the return flow and friction as

$$f[\bar{v}] \approx [\bar{F_x}]. \tag{20}$$

Integrating Eq. (18) vertically from the top of the atmosphere to the bottom boundary, the Coriolis term vanishes due to mass continuity, and the vertically integrated eddy momentum flux convergence is balanced by the vertically integrated friction as

$$-\frac{1}{a\cos^2\phi}\frac{\partial}{\partial\phi}\int_0^{p_s}[\overline{u'v'}]\cos^2\phi\, dp \approx \int_0^{p_s}[\bar{F_x}]dp, \tag{21}$$

where p_s denotes surface pressure. It is clear from (21) that the role of the Ferrel cell is to transfer the momentum forcing between the upper and lower atmosphere while it does not change the vertically integrated zonal momentum budget.

In the limit of vanishing friction, Eq. (20) no longer holds while the Ferrel cell still exists. So how can the Coriolis term of the return flow be balanced? Within the small Rossby number regime where Eq. (18) holds, the Coriolis term of the return flow in the lower atmosphere must be balanced by the eddy momentum flux convergence similar to the upper atmosphere but with the opposite sign. From Earth-like and Jupiter-like simulations shown in Fig. 11 and 12, we can see that this is indeed the case. In the upper atmosphere, eddies converge momentum into the westerly jets as in Earth's atmosphere. However, in the lower atmosphere, eddies diverge momentum out of the westerly jets when bottom friction is low enough. For the Earth-like simulation with the smallest bottom friction, the eddy momentum flux develops a somewhat more complicated vertical structure, with multiple sign reversals–consistent with the more complicated structure of the zonal-mean overturning circulation in Fig. 8. Nevertheless, the general picture of momentum flux into the westerly jet in the upper atmosphere and out of the jet near the surface remains.

It is natural to ask whether the unusual vertical structure of the momentum flux is a result of vertically coherent eddies or separate eddies in the upper and lower atmosphere. A useful tool to characterize the disturbances is the cospectra diagnostic developed by Hayashi (1973, 1982), Randel and Held (1991), and Wheeler and Kiladis (1999). We diagnosed eddy momentum flux cospectra as a function of latitude for the Earth-like simulations with $\tau_f = 1$ and $\tau_f = 10^3$ days. The upper-troposphere cospectrum for the Earth-like control run ($\tau_f = 1$ day) shows the familiar feature of Earth's atmosphere–that the eddy momentum flux is almost confined within the critical latitude $\bar{u} = c$ (Fig. 13 top). For the simulation with $\tau_f = 10^3$ days, the eddy momentum flux peaks at a phase speed of about -20 m/s, both for the upper and lower atmospheres (Fig. 13 middle and bottom). The similar phase speeds indicate that the waves are vertically coherent in the upper and lower atmosphere rather than two separate waves. A big difference compared to the control run ($\tau_f = 1$ day) is that the waves are propagating westwards instead of eastwards. As a result, the waves do not have a critical latitude in the upper atmosphere. Therefore, wave breaking is strongly suppressed compared with the control run, which leads to a reduction of eddy diffusivity and thus a reduction of heat flux (Nakamura 2004). As EKE generation rate is proportional to heat flux, a suppression of wave breaking may also explain why EKE generation is much smaller in the low friction runs. The reason for waves to propagate westwards is that the waves have a very long wavelength. The eddy momentum flux almost exclusively results from a zonal wavenumber 3 wave, which is evidently the dominant wavenumber seen from the snapshot of Ertel's potential vorticity (Fig. 4). In the lower atmosphere momentum fluxes peak at the critical level, and are directed from the westerly into the easterly jet (down-gradient). The momentum fluxes in the lower atmosphere thus resemble characteristics of barotropic instability–although the time- and zonal-mean flow does not show a reversal of the absolute vorticity gradient (not shown).

In the Jupiter-like simulations, the waves that contribute to opposite momentum fluxes in the upper and lower atmosphere seem to be somewhat less coherent in the vertical. Fig. 14 shows that waves in the lower atmosphere seem to move faster towards the west than those in the upper atmosphere for $\tau_f = 5000$ days simulation. Moreover the momentum fluxes are not as clearly dominated by a single wave with a well defined phase speed. Although the waves move westward, they still encounter a critical latitude in the upper troposphere. In the lower atmosphere, momentum fluxes again peak near the critical latitudes and are directed from the westerly into the easterly regions–resembling properties of barotropic instability. Down-gradient momentum fluxes are consistent with the spectral EKE budget in Fig. 10, which shows a conversion from ZKE to EKE at large scales. Primary mode analysis similar as above shows that vertically coherent waves also have opposite momentum fluxes in the upper and lower atmosphere, however, they only contribute to part of the momentum fluxes in the lower atmosphere.

The exact mechanism that leads to the reversed momentum fluxes in the lower atmosphere remains unclear, and may differ between the Earth-like and Jupiter-like simulations. However, two robust properties emerge: 1) lower-atmospheric poleward heat fluxes shift into the easterly jet regions (Figs. 2 and 3), and 2) lower-atmospheric momentum fluxes are down-gradient and peak near the critical latitudes (Figs. 13 and 14). Together, these observations suggest that wave generation in the lower atmosphere shifts into the easterly jet regions, and is possibly caused by a mixed baroclinic-barotropic instability. An analysis of Ertel's PV (not shown), reveals no clear reversals of the PV gradient along isentropes within the atmosphere, though the analysis is complicated by the large variations in surface pressure, and we note that flow characteristics may be impacted significantly by non-QG effects. In either case, the processes that govern momentum flux and mixing in the limit of very low bottom friction demand further investigation, which may profit from more idealized simulations.

d. Dynamical convergence with respect to hyperviscosity and bottom friction

In our low friction limit, although most of EKE generation is "recycled", a small remainder is balanced by the hyperviscosity. Hyperviscosity itself is often regarded as a numerical device to prevent energy or enstrophy from building up at grid scales and it does not directly represent any physical processes. However, all real fluids have a viscosity that removes energy or enstrophy, according to the situation, and it is common in numerical models to use hyperviscosity instead of a true viscosity because it achieves a greater scale-selectivity. In turbulent flows, the energy dissipation (or enstrophy dissipation in quasi-two-dimensional flow) becomes independent of the viscosity if the viscosity is small enough. Analogously, in our simulations we expect that the dynamics of the energy containing scales, and the dissipation itself, should ideally become independent of the hyperviscosity if the latter is small enough. However, this does not mean that the hyperviscous dissipation itself need be small, and in the limit of small bottom friction it can be expected to dominate over the dissipation due to bottom friction.

To explore these expectations, Earth-like simulations with T127 resolution are carried out for all values of τ_f from 1 to 10^4 days, and at T213 resolution, with a lower hyperviscosity, for τ_f equal to 10^3 days. By varying τ_f we explore the convergence with respect to bottom friction, and by varying the resolution we explore convergence with respect to hyperviscosity (and resolution). In any given simulation we keep the damping time scale for the smallest waves the same as resolution varies, so that hyperviscosity decreases by a factor of about 3^8 in the T127 simulations relative to the T42 simulations, with a larger factor still in the T213 simulations. Generally speaking, T127 simulations have similar energy budgets (Fig. 15) and momentum budgets (Fig. 16) as the T42 simulations when friction is reduced towards zero, which confirms at least that the energy recycling and momentum reversal are robust mechanisms that enable the flow to equilibrate in the low friction limit.

Now consider convergence with respect to hyperviscosity. There are in fact some small differences at the lowest values of bottom drag, as is apparent by comparing Figs. 11 and 16. For $\tau_f = 1$ day, the jet strength and momentum fluxes are very similar between T42 and T127 runs, but for $\tau_f = 10^3$ days and 10^4 days , the jets and momentum fluxes are a little stronger in T127 runs. This is seen more clearly from the KE and EKE spectra of different resolution runs with $\tau_f = 1$ day (Fig. 17) and $\tau_f = 10^3$ days (Fig. 18). However, the basic picture of energy recycling remains largely the same (Figs. 7 and 15). At still higher resolution, T213, the simulation with $\tau_f = 10^3$ days also shows very similar KE and EKE spectra to the T127 run for wavenumbers smaller than

60 (Fig. 18), which suggests that the synoptic-scale flow essentially converges when the resolution is beyond T127.

As regards convergence with respect to bottom friction, lowering the bottom drag from $\tau_f = 10^3$ days to $\tau_f = 10^4$ days produces only a small change in the energy spectrum at T127 (Fig. 20). The total total energy budget in Fig. 15 shows an increasing energy dissipation rate by hyperviscosity at $\tau_f = 10^3$ days and $\tau_f = 10^4$ days. The spectral energy budget (Fig. 21) reveals that this increasing dissipation primarily balances increasing generation of EKE near the grid scale, which appears to be associated with grid-scale convection (compare also Schneider and Liu 2009; Liu and Schneider 2010, 2011, 2015). As EKE generated by grid-scale convection does not cascade to larger scales, the effect of this grid-scale convection on the synoptic-scale flow is likely to be small. Comparing the spectral kinetic energy budget for $\tau_f = 10^3$ and $\tau_f = 10^4$ (Fig. 21) also reveals some changes at larger scales, suggesting that true convergence has not been reached, but the main features remain robust. These results suggest that the two cases with smallest drag are indeed in a low bottom-friction regime and that further reducing the drag would likely only have a quantitative effect. Although we cannot claim to have achieved true convergence with respect to either bottom drag or hyperviscosity, the evidence of our simulations suggests that further reducing the drag, or the hyperviscosity, would affect the energy budget only in relatively minor ways.

4. Discussions and Conclusions

In this paper, we have explored the possibility of a baroclinic atmosphere to equilibrate close to the limit of vanishing bottom friction. By reducing bottom friction to extremely low values in a primitive equation model, we found that the baroclinic turbulence can adjust its energy and momentum budgets in order to equilibrate.

- *Energy budget.* Near the Rossby deformation radius, the eddies convert potential energy to eddy kinetic energy similar to Earth's atmosphere. Eddy kinetic energy inversely cascades to larger scales or gets channeled into zonal jets. At the largest scales, kinetic energy is converted back into potential energy, thus closing the kinetic energy cycle without requiring significant dissipation. The total kinetic energy generation for the whole flow is strongly reduced, and thus can be balanced by hyperviscosity dissipation.

- *Momentum budget.* The vertically integrated eddy momentum flux convergence is close to zero as there is no bottom friction to balance it. In the upper atmosphere, eddies converge momentum into the westerly jets similar to Earth's atmosphere. However, in the lower atmosphere, the momentum flux reverses sign and diverges momentum *out* of the westerly jets. A Ferrel cell like circulation balances the zonal flow acceleration/deceleration by the momentum flux convergence/divergence, and thus at the same time converts kinetic energy into potential energy.

The entropy budget in Appendix C shows a consistent picture with the total kinetic energy budget, and it confirms that the energy "recycling" mechanism does not violate the third law of thermodynamics. Close to the vanishing friction limit, radiative forcing acts as the entropy sink, similar to but much smaller than in Earth's atmosphere, and the major entropy source is hyperviscosity. In addition, it confirms that hyperdiffusion on the temperature field is not important in dissipating entropy, and thus potential energy (Lapeyre and Held 2003).

The above budgets are robust in a dry primitive equation model with different planetary parameters and different resolutions. The fact that eddy kinetic energy generated by baroclinic instability can be converted back into potential energy at the largest scales takes away the burden from the friction to dissipate kinetic energy, and thus a significant energy cycle with finite zonal wind can be maintained even when the friction is extremely small. Further reducing surface friction or hyperviscosity seems to only affect the energy budget in relatively minor ways. Therefore, we believe that a baroclinic atmosphere described by the dry primitive equation model could equilibrate with finite velocity close to the limit of vanishing friction. Indeed, simulations without bottom friction do equilibrate, though we have not studied their dynamical convergence with resolution in detail. Also, these simulations inevitably depend on the initial conditions. For the Jupiter-like simulation we even saw a dependence on the initial conditions at finite, but very low, friction (τ_f=5000 days). The kinetic energy generation is very large when the model spins up and multiple jets form quickly. Once jets form, the kinetic energy generation rate becomes smaller and the flow becomes less turbulent. However, at model spin-up, the jets are less stable and can merge randomly. Due to the chaotic jet merging, the model can equilibrate in a non- hemispherically-symmetric state with a different number of jets in the Northern and Southern hemispheres. However, if we initialize the run from the end of the $\tau_f = 50$ days run, where the kinetic energy generation rate is already small and jets are already stable, the flow equilibrates in a hemispherically-symmetric state, which is used in this paper.

Returning to the hypotheses we proposed in the introduction, our results suggest a mixture of hypothesis 2 and 3 to be in effect. When friction reduces, we first get a strong reduction of EKE generation (in agreement with hypothesis 2) but then EKE generation plateaus and we get energy "recycling" (more consistent with hypothesis 3). Although small-scale disturbances become more energetic and more ageostrophic effects may come into play at smallest scales, dissipation by hyperviscosity is never dominant in the EKE budget, and we do not see a significant increase in downscale energy transfer. Therefore, hypothesis 1 is less favored.

The limit of vanishing bottom friction may be relevant for atmospheres where the frictional time scale is much much larger than the radiative forcing time scale, perhaps the Jovian atmosphere.

Indirect evidence that may relate them is the kinetic energy spectrum, shown in Fig. 22. The zonal kinetic energy spectrum seems to have a range with approximately -5 slope for either large ($\tau_f = 5$ days) or very small ($\tau_f = 5000$ days) friction, and the eddy kinetic energy spectrum has a slope slightly steeper than -5/3. At large friction, the zonal jets and eddies have similar scales and energy levels. However, when friction is very small, the zonal flow extends to larger scales than the eddies, and it contains much more energy than the eddies. Therefore, the total flow is dominated by the strong and slowly evolving zonal jets on the largest scale and the spectrum seems to follow a k^{-5} slope within wavenumbers 20 to 50, consistent with the zonostrophic turbulence regime (Sukoriansky et al. 2002; Galperin et al. 2006, 2014). At small scales, on the other hand, the spectrum is dominated by isotropic turbulence with a spectral slope near $k^{-5/3}$. These features resemble Jupiter's magnificent jets.

Acknowledgments. We thank Isaac Held and Pablo Zurita-Gotor for helpful comments and discussions. We also thank Zhaoyi Shen for carefully reading the manuscript. The numerical simulations were performed on GFDL's computer system. This work was funded by the NSF under grant AGS-1144302 and the NOAA under grant NA08OAR4320752. The statements, findings, conclusions, and recommendations are those of the authors and do not necessarily reflect the views of the NSF, the NOAA, or the U.S. Department of Commerce.

APPENDIX A

Lorenz Energy Cycle Formulation

The Lorenz energy cycle used in our calculations mostly follows the original formulation of Lorenz (1955) and Peixto and Oort (1984). The EKE and ZKE are defined as energy per unit surface area written as

$$\text{EKE} = \frac{1}{2}\int \mathbf{u}'^2 dm, \tag{A1}$$

$$\text{ZKE} = \frac{1}{2}\int \overline{\mathbf{u}}^2 dm, \tag{A2}$$

where $\mathbf{u}$ is the horizontal velocity vector. $\overline{A}$ and A' denote the zonal average of A and deviations from the zonal average, respectively. $\int dm$ denotes a mass-weighted global integral:

$$\int dm = \frac{1}{4\pi g}\int_0^{2\pi} d\lambda \int_0^{\pi} \cos\phi d\phi \int_0^{p_0} dp. \tag{A3}$$

Therefore, the unit for EKE and ZKE is J m^{-2}. The energy conversion between potential and kinetic energy is evaluated as

$$C(\text{PE}, \text{EKE}) = -R\int p^{-1}\omega' T' dm, \tag{A4}$$

and

$$C(\text{PE}, \text{ZKE}) = -R\int p^{-1}\overline{\omega}\overline{T} dm, \tag{A5}$$

where R is the gas constant, $\omega = dp/dt$, and T is temperature. The energy transfer between eddy and zonal mean kinetic energy is evaluated as

$$C(\text{EKE}, \text{ZKE}) \approx \int \cos\phi \left(\overline{u'v'}\frac{\partial}{a\partial\phi} + \overline{u'\omega'}\frac{\partial}{\partial p}\right)\left(\frac{\overline{u}}{\cos\phi}\right) dm. \tag{A6}$$

Note that we have neglected terms involving $\overline{v}$, which are inevitably small.

APPENDIX B

Spectral Kinetic Energy Budget in σ-coordinates

The kinetic energy per unit surface area (and eddy kinetic energy in a similar way) in $\sigma-$coordinates can be written as

$$\text{KE} = \int ds \int_0^1 d\sigma \left(\frac{1}{2}p_s \mathbf{u}^2\right), \tag{B1}$$

where p_s is the surface pressure and the integral

$$\int ds = \frac{1}{4\pi g}\int_0^{2\pi} d\lambda \int_0^{\pi} \cos\phi d\phi. \tag{B2}$$

To approximate (B1) into a quadratic form, we must substitute p_s by its mean value $\bar{p}_s$ and obtain

$$\mathrm{KE} \approx \bar{p}_s \int ds \int_0^1 d\sigma \left(\frac{1}{2}\mathbf{u}^2\right). \tag{B3}$$

The horizontal velocity field on the sphere can be decomposed into vortical part and divergent part as $\mathbf{u} = \mathbf{u}_{vor} + \mathbf{u}_{div}$, where $\nabla \times \mathbf{u}_{vor} = \zeta$ and $\nabla^2\psi = \zeta$ (ζ is relative vorticity and ψ is the stream function). The divergent part of the flow is much smaller than the vortical flow and it is safe to ignore it in the kinetic energy. Eq. (B3) becomes

$$\begin{aligned}
\mathrm{KE} &\approx \bar{p}_s \int ds \int_0^1 d\sigma \left(\frac{1}{2}\mathbf{u}_{vor}^2\right) && \text{(B4)}\\
&= \bar{p}_s \int ds \int_0^1 d\sigma \left(-\frac{1}{2}\psi\nabla^2\psi\right) = \bar{p}_s \int ds \int_0^1 d\sigma \left(-\frac{1}{2}\psi\zeta\right) && \text{(B5)}\\
&= -\frac{1}{4}\bar{p}_s g^{-1} \int_0^1 d\sigma \sum_{n,m} \{\psi\}^*_{n,m} \{\zeta\}_{n,m}, && \text{(B6)}
\end{aligned}$$

where $\{\}_{n,m}$ denotes the spectrum component of the fields with total wavenumber n and zonal wavenumber m. As stream function and relative vorticity are related in spectral space by

$$\{\zeta\}_{n,m} = -\frac{n(n+1)}{a^2}\{\psi\}_{n,m}, \tag{B7}$$

where a is the planetary radius, (B6) becomes

$$\mathrm{KE} \approx \frac{1}{4}\bar{p}_s g^{-1} \int_0^1 d\sigma \sum_n \sum_{m=-n}^{n} \frac{a^2}{n(n+1)} \{\zeta\}^*_{n,m}\{\zeta\}_{n,m}, \tag{B8}$$

and kinetic energy within one wavenumber

$$\mathrm{KE}_n \approx \frac{1}{4}\bar{p}_s g^{-1} \int_0^1 d\sigma \sum_{m=-n}^{n} \frac{a^2}{n(n+1)} \{\zeta\}^*_{n,m}\{\zeta\}_{n,m}. \tag{B9}$$

The kinetic energy budget can now be derived from the evolution equation for vorticity

$$
\begin{aligned}
\frac{\partial \zeta}{\partial t} &= -(f+\zeta)\nabla\cdot\mathbf{u} - \mathbf{u}\cdot\nabla f - \mathbf{u}\cdot\nabla\zeta - R\nabla T\times\nabla\ln p_s - \nabla\times\left(\dot{\sigma}\frac{\partial\mathbf{u}}{\partial\sigma}\right) - d_{fri} - d_{vis} \\
&\approx -(f+\zeta)\nabla\cdot\mathbf{u}_{div} - \mathbf{u}_{vor}\cdot\nabla f - \mathbf{u}_{vor}\cdot\nabla\zeta - R\nabla T\times\nabla\ln p_s - \nabla\times\left(\dot{\sigma}\frac{\partial\mathbf{u}}{\partial\sigma}\right) - d_{fri} - d_{vis}
\end{aligned} \tag{B10}
$$

where d_{fri} and d_{vis} denote damping by friction and hyperviscosity respectively. Transforming (B10) into spectral space and multiplying it by $\{\zeta\}^*_{n,m}$ leads to the spectral kinetic energy budget. Energy transfer from all other wavenumbers into wavenumber n by nonlinear interactions is computed as

$$
T^n_{NL} = \frac{1}{2}\bar{p}_s g^{-1}\frac{a^2}{n(n+1)}\int_0^1 d\sigma\sum_{m=-n}^{n}\{\zeta\}^*_{n,m}\{-\mathbf{u}_{vor}\cdot\nabla\zeta\}_{n,m}, \tag{B11}
$$

which vanishes upon summation over all wavenumbers. Kinetic energy generation at wavenumber n is computed as

$$
G^n_{KE} = \frac{1}{2}\bar{p}_s g^{-1}\frac{a^2}{n(n+1)}\int_0^1 d\sigma\sum_{m=-n}^{n}\{\zeta\}^*_{n,m}\left\{-(f+\zeta)\nabla\cdot\mathbf{u}_{div} - \mathbf{u}_{vor}\cdot\nabla f - R\nabla T\times\nabla\ln p_s - \nabla\times\left(\dot{\sigma}\frac{\partial\mathbf{u}}{\partial\sigma}\right)\right\} \tag{B12}
$$

where the largest contribution comes from the $f\nabla\cdot\mathbf{u}_{div}$ term, which can be shown to be related to the usual kinetic energy generation term, ωT, in pressure coordinates[3]. The second largest term is $-R\nabla T\times\nabla\ln p_s$, which is unique to the $\sigma-$coordinates. $-\mathbf{u}_{vor}\cdot\nabla f$ is actually a spectral flux by the Coriolis force, which does no net work and is not important in our simulations. The energy dissipation by friction and hyperviscosity are

$$
D^n_{fri} = \frac{1}{2}\bar{p}_s g^{-1}\frac{a^2}{n(n+1)}\int_0^1 d\sigma\sum_{m=-n}^{n}\{\zeta\}^*_{n,m}\{-d_{fri}\}_{n,m}, \tag{B13}
$$

and

$$
D^n_{vis} = \frac{1}{2}\bar{p}_s g^{-1}\frac{a^2}{n(n+1)}\int_0^1 d\sigma\sum_{m=-n}^{n}\{\zeta\}^*_{n,m}\{-d_{vis}\}_{n,m}, \tag{B14}
$$

---

[3]Geostrophic balance is assumed so that $-f\frac{a^2}{n(n+1)}\{\zeta\}^*_{n,m}\sim\{\Psi\}^*_{n,m}$ where Ψ is the geopotential height. Assuming surface pressure is nearly constant so that $\nabla\cdot\mathbf{u}_{div}\sim-\frac{\partial\omega}{\partial p}$. Then the column integral $\int_0^{p_s}-\{\Psi\}^*_{n,m}\frac{\partial\{\omega\}_{n,m}}{\partial p}dp$ approximates $\int_0^{p_s}-\frac{R}{p}\{\omega\}_{n,m}\{T\}^*_{n,m}dp$ if ω vanishes in the upper and lower boundaries.

respectively. When time averaged, The sum of the four terms should be close to zero, and a residual term is included to close the energy budget.

The eddy kinetic energy budget can be formulated by discarding zonal wavenumber 0 in (B10) and further decompose (B11) into eddy-eddy transfer

$$T_{EE}^{n} = \frac{1}{2}\bar{p}_s g^{-1} \frac{a^2}{n(n+1)} \int_0^1 d\sigma \sum_{m=-n,\ m\neq 0}^{n} \{\zeta\}_{n,m}^{*} \{-\mathbf{u}'_{vor} \cdot \nabla\zeta'\}_{n,m}, \tag{B15}$$

and eddy/mean-flow transfer

$$T_{EM}^{n} = \frac{1}{2}\bar{p}_s g^{-1} \frac{a^2}{n(n+1)} \int_0^1 d\sigma \sum_{m=-n,\ m\neq 0}^{n} \{\zeta\}_{n,m}^{*} \{-\bar{\mathbf{u}}_{vor} \cdot \nabla\zeta' - \mathbf{u}'_{vor} \cdot \nabla\bar{\zeta}\}_{n,m}. \tag{B16}$$

APPENDIX C

Entropy budget

Atmospheric motion is often compared to a heat engine to which the first and second laws of thermodynamics can be applied. The first law of thermodynamics states that energy conversion between different forms (e.g., internal, potential and kinetic energy) must conserve the total amount of energy. The second law of thermodynamics further constrains the direction of energy conversion, such that the energy can only change from a more to a less usable form. Mathematically, it states that for an isolated system, there exists a state function S which satisfies

$$dS/dt \geq 0, \tag{C1}$$

where S is the entropy. Eq. (C1) means that entropy will increase monotonically until it reaches maximum at thermodynamic equilibrium. The second law of thermal dynamics constrains the maximum kinetic energy that can be generated from a reservoir of internal energy, and has been applied to various scales of terrestrial atmospheric motions ranging from moist convection (Rennó and Ingersoll 1996; Emanuel and Bister 1996), dust devils (Rennó et al. 1998), hurricane dynamics (Emanuel 1986; Bister and Emanuel 1998), to the general circulation (Barry et al. 2002).

Clearly on the global scale, Earth's atmosphere is not an isolated system, otherwise it would be in a thermodynamical equilibrium state with uniform temperature everywhere. Instead, Earth's atmosphere is an open system due to constant heating from the Sun. The second law can be extended to such an open system using that

$$\frac{dS}{dt} = \int \frac{\dot{Q}}{T} dm + \frac{dS_{irr}}{dt}, \tag{C2}$$

where $\dot{Q}$ is the radiative heating rate per unit mass, T is temperature, $\int dm$ is mass-weighted global integral defined in (A3), and dS_{irr} is the entropy production from irreversible processes (Pauluis and Held 2002). The atmosphere is heated in the tropics where it is warm (T is large), and is cooled in high latitudes where it is cold (T is small), therefore the external heating acts as an entropy sink ($\int \frac{\dot{Q}}{T} dm < 0$). In our idealized dry GCM, the only physical irreversible process is the bottom friction. Additional irreversible processes arise from hyperviscosity on the velocity field and hyperdiffusion on the temperature field. The entropy production from irreversible processes can be evaluated from the associated diabatic heating:

$$\begin{aligned} \frac{dS_{irr}}{dt} &= \int \frac{\dot{Q}_{irr}}{T} dm \\ &= \int \frac{\dot{Q}_f + \dot{Q}_{hyper,v} + \dot{Q}_{hyper,T}}{T} dm, \end{aligned}$$

where $\dot{Q}_f$,$\dot{Q}_{hyper,v}$ and $\dot{Q}_{hyper,T}$ represent diabatic heating resulting from friction, hyperviscosity on velocity and hyperdiffusion on temperature, respectively. For frictional heating, the associated entropy production is

$$\int \frac{\dot{Q}_f}{T} dm = \int \frac{\Gamma : \nabla \mathbf{v}}{T} dm, \tag{C3}$$

where Γ is the stress tensor and $\mathbf{v}$ is the wind velocity. As we used Rayleigh damping to represent friction, (C3) can be further reduced to

$$\int \frac{\dot{Q}_f}{T} dm = \int \frac{k(\sigma)\mathbf{v}^2}{T} dm, \tag{C4}$$

where $k(\sigma)$ is defined in Eq.(2). Similarly, we can evaluate the entropy productions from hyperviscosity and hyperdiffusion.

In a statistically steady state, the entropy sink from external heating must be balanced by the sum of various entropy sources, written as

$$0 = \left[\int \frac{\dot{Q}}{T} dm\right] + \left[\int \frac{\dot{Q}_f}{T} dm\right] + \left[\int \frac{\dot{Q}_{hyper,v}}{T} dm\right] + \left[\int \frac{\dot{Q}_{hyper,T}}{T} dm\right], \tag{C5}$$

where the square brackets denote time averaging. Fig. 23 shows each term in (C5) from the Earth-like simulations with different values of bottom friction. For the control run ($\tau_f = 1$ day), the major entropy production to balance the entropy sink is the bottom friction, while the entropy production from hyperviscosity is negligible. When bottom friction first decreases, both the entropy sink and the frictional entropy production decrease ($\tau_f = 10,\ 10^2$ day), and they nearly balance each other. When bottom friction further decreases, the entropy production by friction continues to decrease, while the entropy sink stays nearly constant and is mainly balanced by entropy production from hyperviscosity ($\tau_f = 10^3,\ 10^4$ day). The entropy production from hyperdiffusion negligible for all τ_f. The entropy budget is similar for the T127 runs. Close to the vanishing friction limit, the hyperviscosity becomes the the dominate entropy source, which in reality may correspond to three-dimensional turbulence at small scales.

References

Barry, L., G. C. Craig, and J. Thuburn, 2002: Poleward heat transport by the atmospheric heat engine. *Nature*, **415 (6873)**, 774–7, doi:10.1038/415774a.

Bister, M., and K. A. Emanuel, 1998: Dissipative heating and hurricane intensity. *Meteor. Atmos. Phys.*, **65 (3-4)**, 233–240, doi:10.1007/BF01030791.

Boffetta, G., and R. E. Ecke, 2012: Two-Dimensional Turbulence. *Annu. Rev. Fluid Mech.*, **44 (1)**, 427–451, doi:10.1146/annurev-fluid-120710-101240.

Chai, J., and G. K. Vallis, 2014: The Role of Criticality on the Horizontal and Vertical Scales of Extratropical Eddies in a Dry GCM. *J. Atmos. Sci.*, **71 (7)**, 2300–2318, doi:10.1175/JAS-D-13-0351.1.

Chen, G., and A. Plumb, 2014: Effective Isentropic Diffusivity of Tropospheric Transport. *J. Atmos. Sci.*, **71 (9)**, 3499–3520, doi:10.1175/JAS-D-13-0333.1.

Chertkov, M., C. Connaughton, I. Kolokolov, and V. Lebedev, 2007: Dynamics of Energy Condensation in Two-Dimensional Turbulence. *Phys. Rev. Lett.*, **99 (8)**, 084 501, doi:10.1103/PhysRevLett.99.084501.

Dowling, T. E., 1995: Dynamics of Jovian Atmospheres. *Annu. Rev. Fluid Mech.*, **27 (1)**, 293–334, doi:10.1146/annurev.fl.27.010195.001453.

Dritschel, D. G., and M. E. McIntyre, 2008: Multiple Jets as PV Staircases: The Phillips Effect and the Resilience of Eddy-Transport Barriers. *J. Atmos. Sci.*, **65 (3)**, 855–874, doi:10.1175/2007JAS2227.1.

Edmon, H. J., B. J. Hoskins, and M. E. McIntyre, 1980: Eliassen-Palm Cross Sections for the Troposphere. *J. Atmos. Sci.*, **37 (12)**, 2600–2616, doi:10.1175/1520-0469(1980)037⟨2600:EPCSFT⟩2.0.CO;2.

Emanuel, K., and M. Bister, 1996: Moist convective velocity and buoyancy scales. *J. Atmos. Sci.*, **53 (22)**, 3276–3285, doi:10.1175/1520-0469(1996)053⟨3276:MCVABS⟩2.0.CO;2.

Emanuel, K. a., 1986: An Air-Sea Interaction Theory for Tropical Cyclones. Part I: Steady-State Maintenance. *J. Atmos. Sci.*, **43 (6)**, 585–605, doi:10.1175/1520-0469(1986)043⟨0585:AASITF⟩2.0.CO;2.

Frierson, D. M. W., I. M. Held, and P. Zurita-Gotor, 2007: A Gray-Radiation Aquaplanet Moist GCM. Part II: Energy Transports in Altered Climates. *J. Atmos. Sci.*, **64 (5)**, 1680–1693, doi:10.1175/JAS3913.1.

Galperin, B., S. Sukoriansky, N. Dikovskaya, P. L. Read, Y. H. Yamazaki, and R. Wordsworth, 2006: Anisotropic turbulence and zonal jets in rotating flows with a beta-effect. *Nonlinear Proc. Geophys.*, **13 (1)**, 83–98, doi:10.5194/npg-13-83-2006.

Galperin, B., R. M. B. Young, S. Sukoriansky, N. Dikovskaya, P. L. Read, A. J. Lancaster, and D. Armstrong, 2014: Cassini observations reveal a regime of zonostrophic macroturbulence on Jupiter. *Icarus*, **229**, 295–320, doi:10.1016/j.icarus.2013.08.030.

Green, J. S. A., 1970: Transfer properties of the large-scale eddies and the general circulation of the atmosphere. *Q. J. R. Meteorol. Soc.*, **96**, 157–185, doi:10.1002/qj.49709741422.

Guillot, T., 2005: The Interiors of Giant Planets: Models and Outstanding Questions. *Annu. Rev. Earth Planet. Sci.*, **33 (1)**, 493–530, doi:10.1146/annurev.earth.32.101802.120325.

Hayashi, Y., 1973: A Method of Analyzing Transient Waves by Space-Time Cross Spectra. *J. Appl. Meteor.*, **12 (2)**, 404–408, doi:10.1175/1520-0450(1973)012⟨0404:AMOATW⟩2.0.CO;2.

Hayashi, Y., 1982: Space-time spectral analysis and its applications to atmospheric waves. *J. Meteorol. Soc. Jpn.*, **60 (1)**, 156–171.

Haynes, P. H., and M. E. McIntyre, 1987: On the Evolution of Vorticity and Potential Vorticity in the Presence of Diabatic Heating and Frictional or Other Forces. *J. Atmos. Sci.*, **44 (5)**, 828–841, doi:10.1175/1520-0469(1987)044⟨0828:OTEOVA⟩2.0.CO;2.

Held, I. M., 1975: Momentum Transport by Quasi-Geostrophic Eddies. *J. Atmos. Sci.*, **32 (7)**, 1494–1497, doi:10.1175/1520-0469(1975)032⟨1494:MTBQGE⟩2.0.CO;2.

Held, I. M., 2007: Progress and problems in large-scale atmospheric dynamics. *The Global Circulation of the Atmosphere*, T. Schneider, and A. Sobel, Eds., Princeton University Press, Princeton, NJ, chap. 1, 1–21.

Held, I. M., and V. D. Larichev, 1996: A Scaling Theory for Horizontally Homogeneous, Baroclinically Unstable Flow on a Beta Plane. *J. Atmos. Sci.*, **53 (7)**, 946–952, doi:10.1175/1520-0469(1996)053⟨0946:ASTFHH⟩2.0.CO;2.

Held, I. M., and M. J. Suarez, 1994: A Proposal for the Intercomparison of the Dynamical Cores of Atmospheric General Circulation Models. *Bull. Amer. Meteor. Soc.*, **75 (10)**, 1825–1830, doi:10.1175/1520-0477(1994)075⟨1825:APFTIO⟩2.0.CO;2.

Ingersoll, A. P., 1990: Atmospheric dynamics of the outer planets. *Science*, **248 (4953)**, 308–15, doi:10.1126/science.248.4953.308.

James, I. N., 1987: Suppression of Baroclinic Instability in Horizontally Sheared Flows. *J. Atmos. Sci.*, **44 (24)**, 3710–3720, doi:10.1175/1520-0469(1987)044⟨3710:SOBIIH⟩2.0.CO;2.

James, I. N., and L. J. Gray, 1986: Concerning the effect of surface drag on the circulation of a baroclinic planetary atmosphere. *Q. J. R. Meteorol. Soc.*, **112 (474)**, 1231–1250, doi:10.1002/qj.49711247417.

Jansen, M., and R. Ferrari, 2013: Equilibration of an Atmosphere by Adiabatic Eddy Fluxes. *J. Atmos. Sci.*, **70 (9)**, 2948–2962, doi:10.1175/JAS-D-13-013.1.

Kaspi, Y., and G. R. Flierl, 2007: Formation of Jets by Baroclinic Instability on Gas Planet Atmospheres. *J. Atmos. Sci.*, **64 (9)**, 3177–3194, doi:10.1175/JAS4009.1.

Koshyk, J. N., and K. Hamilton, 2001: The Horizontal Kinetic Energy Spectrum and Spectral Budget Simulated by a High-Resolution Troposphere-Stratosphere-Mesosphere GCM. *J. Atmos. Sci.*, **58 (4)**, 329–348, doi:10.1175/1520-0469(2001)058⟨0329:THKESA⟩2.0.CO;2.

Kraichnan, R. H., 1967: Inertial Ranges in Two-Dimensional Turbulence. *Phys. Fluids*, **10 (7)**, 1417, doi:10.1063/1.1762301.

Lambert, S. J., 1984: A global available potential energy-kinetic energy budget in terms of the two-dimensional wavenumber for the FGGE year. *Atmos.-Ocean*, **22 (3)**, 265–282, doi:10.1080/07055900.1984.9649199.

Lapeyre, G., and I. M. Held, 2003: Diffusivity, Kinetic Energy Dissipation, and Closure Theories for the Poleward Eddy Heat Flux. *J. Atmos. Sci.*, **60 (23)**, 2907–2916, doi:10.1175/1520-0469(2003)060⟨2907:DKEDAC⟩2.0.CO;2.

Li, L., A. P. Ingersoll, X. Jiang, D. Feldman, and Y. L. Yung, 2007: Lorenz energy cycle of the global atmosphere based on reanalysis datasets. *Geophys. Res. Lett.*, **34**, 1–5, doi:10.1029/2007GL029985.

Lian, Y., and A. P. Showman, 2008: Deep jets on gas-giant planets. *Icarus*, **194 (2)**, 597–615, doi:10.1016/j.icarus.2007.10.014.

Liu, J., and T. Schneider, 2010: Mechanisms of Jet Formation on the Giant Planets. *J. Atmos. Sci.*, **67 (11)**, 3652–3672, doi:10.1175/2010JAS3492.1.

Liu, J., and T. Schneider, 2011: Convective Generation of Equatorial Superrotation in Planetary Atmospheres. *J. Atmos. Sci.*, **68 (11)**, 2742–2756, doi:10.1175/JAS-D-10-05013.1.

Liu, J., and T. Schneider, 2015: Scaling of Off-Equatorial Jets in Giant Planet Atmospheres. *J. Atmos. Sci.*, **72 (1)**, 389–408, doi:10.1175/JAS-D-13-0391.1.

Lorenz, D. J., 2015: Understanding Midlatitude Jet Variability and Change Using Rossby Wave Chromatography: Methodology. *J. Atmos. Sci.*, **72 (1)**, 369–388, doi:10.1175/JAS-D-13-0199.1.

Lorenz, E. N., 1955: Available Potential Energy and the Maintenance of the General Circulation. *Tellus A*, **7**, 157–167, doi:10.3402/tellusa.v7i2.8796.

Mahlman, J. D., 1997: Dynamics of Transport Processes in the Upper Troposphere. *Science*, **276 (5315)**, 1079–1083, doi:10.1126/science.276.5315.1079.

Merlis, T. M., and T. Schneider, 2009: Scales of Linear Baroclinic Instability and Macroturbulence in Dry Atmospheres. *J. Atmos. Sci.*, **66 (6)**, 1821–1833, doi:10.1175/2008JAS2884.1.

Nakamura, N., 2004: Quantifying Asymmetric Wave Breaking and Two-Way Transport. *J. Atmos. Sci.*, **61 (22)**, 2735–2748, doi:10.1175/JAS3296.1.

Pauluis, O., and I. M. Held, 2002: Entropy Budget of an Atmosphere in Radiative-Convective Equilibrium. Part I: Maximum Work and Frictional Dissipation. *J. Atmos. Sci.*, **59 (2)**, 125–139, doi:10.1175/1520-0469(2002)059⟨0125:EBOAAI⟩2.0.CO;2.

Peixto, J. P., and A. H. Oort, 1984: Physics of climate. *Rev. Mod. Phys.*, **56 (3)**, 365–429, doi:10.1103/RevModPhys.56.365.

Polvani, L. M., J. C. McWilliams, M. A. Spall, and R. Ford, 1994: The coherent structures of shallow-water turbulence: Deformation-radius effects, cyclone/anticyclone asymmetry and gravity-wave generation. *Chaos*, **4 (2)**, 177, doi:10.1063/1.166002.

Randel, W. J., and I. M. Held, 1991: Phase speed spectra of transient eddy fluxes and critical layer absorption. *J. Atmos. Sci.*, **48**, 688–697, doi:10.1175/1520-0469(1991)048⟨0688:PSSOTE⟩2.0.CO;2.

Rennó, N. O., M. L. Burkett, and M. P. Larkin, 1998: A Simple Thermodynamical Theory for Dust Devils. *J. Atmos. Sci.*, **55 (21)**, 3244–3252, doi:10.1175/1520-0469(1998)055⟨3244:ASTTFD⟩2.0.CO;2.

Rennó, N. O., and A. P. Ingersoll, 1996: Natural Convection as a Heat Engine: A Theory for CAPE. *J. Atmos. Sci.*, **53 (4)**, 572–585, doi:10.1175/1520-0469(1996)053⟨0572:NCAAHE⟩2.0.CO;2.

Robinson, W. a., 2006: On the Self-Maintenance of Midlatitude Jets. *J. Atmos. Sci.*, **63 (8)**, 2109–2122, doi:10.1175/JAS3732.1.

Schneider, T., and J. Liu, 2009: Formation of Jets and Equatorial Superrotation on Jupiter. *J. Atmos. Sci.*, **66 (3)**, 579–601, doi:10.1175/2008JAS2798.1.

Schneider, T., and C. C. Walker, 2006: Self-Organization of Atmospheric Macroturbulence into Critical States of Weak Nonlinear Eddy-Eddy Interactions. *J. Atmos. Sci.*, **63 (6)**, 1569–1586, doi:10.1175/JAS3699.1.

Scott, R. K., and D. G. Dritschel, 2013: Halting scale and energy equilibration in two-dimensional quasigeostrophic turbulence. *J. Fluid Mech.*, **721**, R4, doi:10.1017/jfm.2013.120.

Showman, A. P., 2007: Numerical Simulations of Forced Shallow-Water Turbulence: Effects of Moist Convection on the Large-Scale Circulation of Jupiter and Saturn. *J. Atmos. Sci.*, **64 (9)**, 3132–3157, doi:10.1175/JAS4007.1.

Showman, A. P., P. J. Gierasch, and Y. Lian, 2006: Deep zonal winds can result from shallow driving in a giant-planet atmosphere. *Icarus*, **182 (2)**, 513–526, doi:10.1016/j.icarus.2006.01.019.

Showman, A. P., and A. P. Ingersoll, 1998: Interpretation of Galileo probe data and implications for Jupiter's dry downdrafts. *Icarus*, **132 (2)**, 205–220, doi:10.1006/icar.1998.5898.

Simon-Miller, A. A., B. J. Conrath, P. J. Gierasch, G. S. Orton, R. K. Achterberg, F. M. Flasar, and B. M. Fisher, 2006: Jupiter's atmospheric temperatures: From Voyager IRIS to Cassini CIRS. *Icarus*, **180 (1)**, 98–112, doi:10.1016/j.icarus.2005.07.019.

Smith, L., and V. Yakhot, 1993: Bose condensation and small-scale structure generation in a random force driven 2D turbulence. *Phys. Rev. Lett.*, **71 (3)**, 352–355, doi:10.1103/PhysRevLett.71.352.

Sukoriansky, S., B. Galperin, and N. Dikovskaya, 2002: Universal spectrum of two-dimensional turbulence on a rotating sphere and some basic features of atmospheric circulation on giant planets. *Phys. Rev. Lett.*, **89 (12)**, 124 501, doi:10.1103/PhysRevLett.89.124501.

Vallis, G. K., 2006: *Atmospheric and Oceanic Fluid Dynamics*. Cambridge University Press, Cambridge, U.K., 745 pp.

Vallis, G. K., and M. E. Maltrud, 1993: Generation of Mean Flows and Jets on a Beta Plane and over Topography. *J. Phys. Oceanogr.*, **23 (7)**, 1346–1362, doi:10.1175/1520-0485(1993)023⟨1346:GOMFAJ⟩2.0.CO;2.

Vasavada, A. R., and A. P. Showman, 2005: Jovian atmospheric dynamics: an update after Galileo and Cassini. *Rep. Prog. Phys.*, **68 (8)**, 1935–1996, doi:10.1088/0034-4885/68/8/R06.

Waite, M. L., and C. Snyder, 2009: The Mesoscale Kinetic Energy Spectrum of a Baroclinic Life Cycle. *J. Atmos. Sci.*, **66**, 883–901, doi:10.1175/2008JAS2829.1.

Wheeler, M., and G. N. Kiladis, 1999: Convectively Coupled Equatorial Waves: Analysis of Clouds and Temperature in the Wavenumber-Frequency Domain. *J. Atmos. Sci.*, **56 (3)**, 374–399, doi:10.1175/1520-0469(1999)056⟨0374:CCEWAO⟩2.0.CO;2.

Williams, G. P., and J. L. Halloway, 1982: The range and unity of planetary circulations. *Nature*, **297 (5864)**, 295–299, doi:10.1038/297295a0.

Williams, P., 1985: *Issues in Atmospheric and Oceanic Modeling - Part A Climate Dynamics*, Advances in Geophysics, Vol. 28. Elsevier.

Zurita-Gotor, P., 2008: The Sensitivity of the Isentropic Slope in a Primitive Equation Dry Model. *J. Atmos. Sci.*, **65 (1)**, 43–65, doi:10.1175/2007JAS2284.1.

LIST OF FIGURES

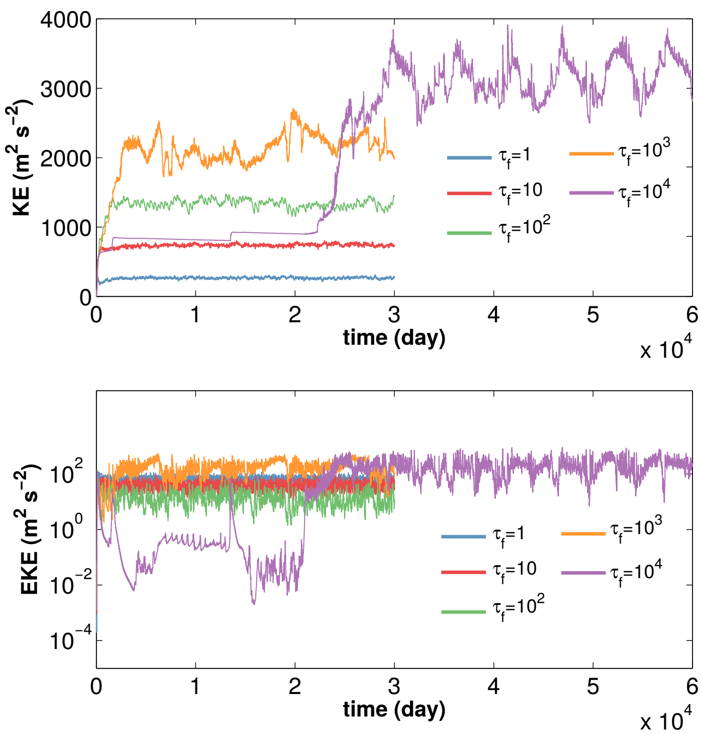

FIG. 1. Evolution of (above) kinetic energy and (below) eddy kinetic energy in the Earth-like simulations with different strength of surface friction.

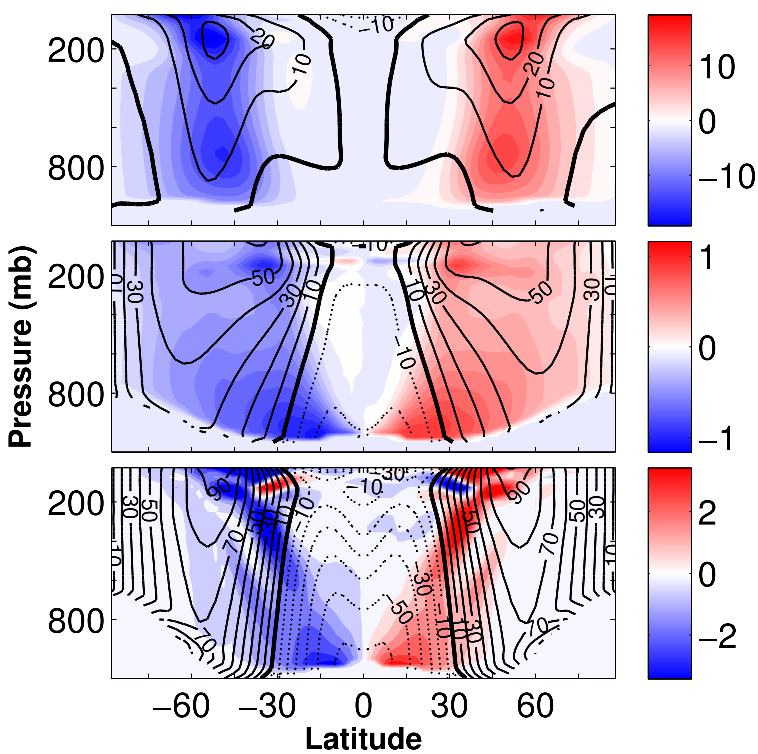

FIG. 2. Zonal and temporal mean zonal wind (contour) and eddy potential temperature flux (color) for Earth-like simulations with different strength of surface friction: τ_f =(top) 1, (middle) 10^2, (bottom) 10^4 days. The contour interval for zonal wind is 10 m/s.

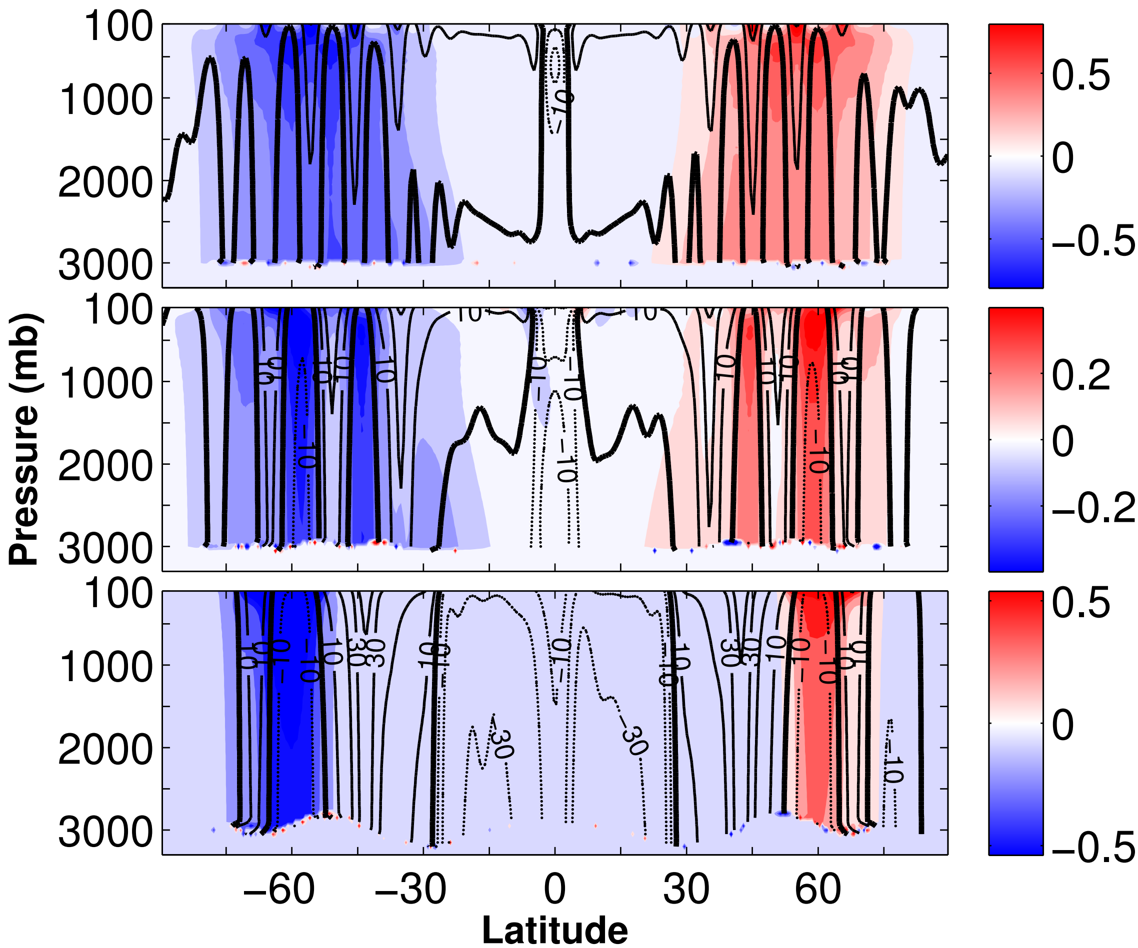

FIG. 3. Zonal and temporal mean zonal wind (contour) and eddy potential temperature flux (color) for Jupiter-like simulations with different strength of surface friction: τ_f =(top) 5, (middle) 50, (bottom) 5000 days. The contour interval for zonal wind is 10 m/s.

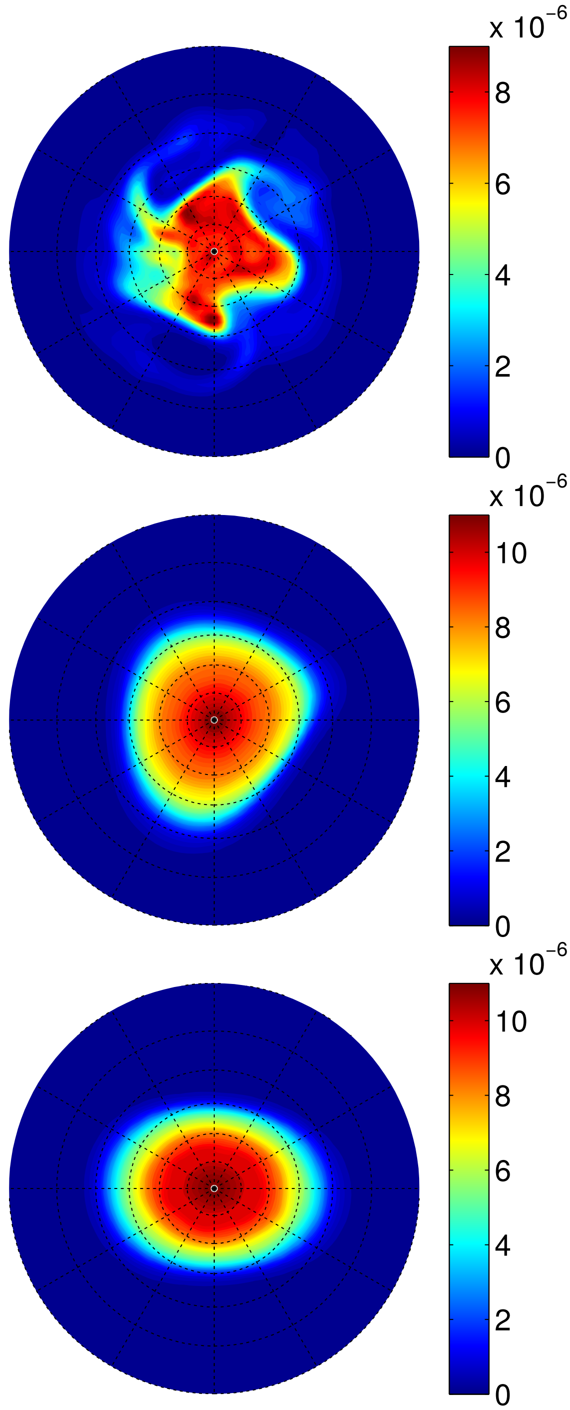

FIG. 4. Instantaneous Ertel's potential vorticity fields on istentropic surface $\theta = 330$ K for Earth-like simulations with different strength of surface friction: $\tau_f =$ (top) 1, (middle) 10^3 and (bottom) 10^4 days. The unit is $\mathrm{m^2\ K\ s^{-1}\ kg^{-1}}$. The whole Norther hemisphere (latitudinal range 0° to 90°) is shown.

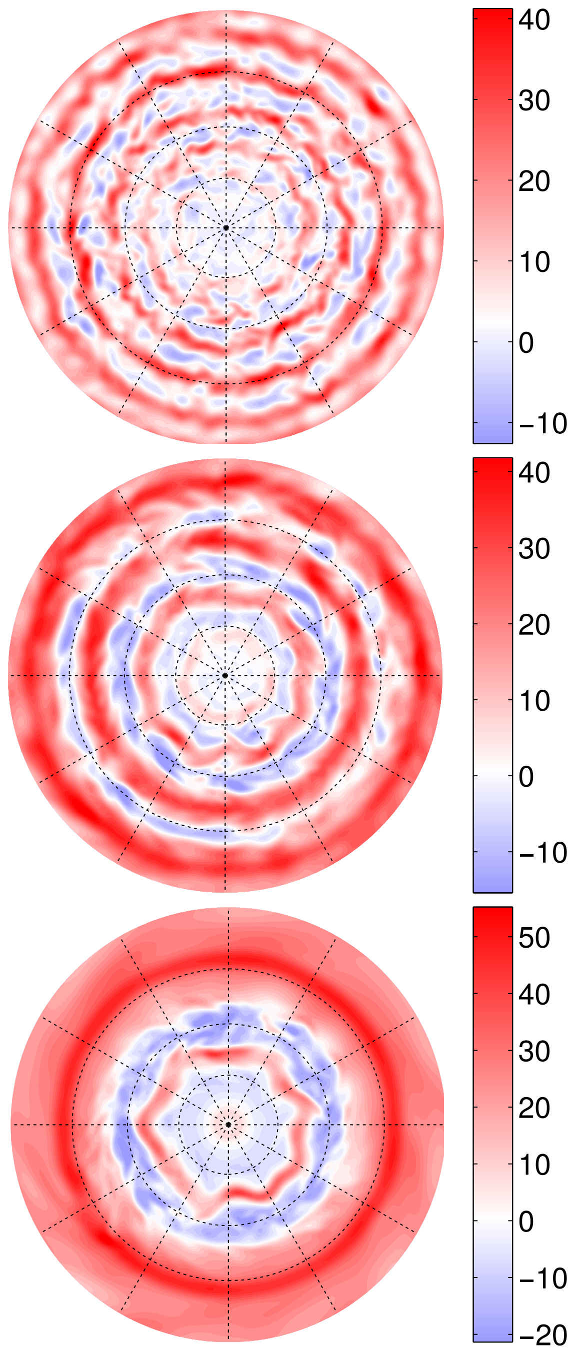

FIG. 5. Instantaneous zonal wind fields in the upper atmosphere (σ =0.02) for Jupiter-like simulations with different strength of surface friction: τ_f = (top) 5, (middle) 50 and (bottom) 5000 days. The unit is m s^{-1}. Only the extratropical region (latitudinal range 30° to 90°) is shown.

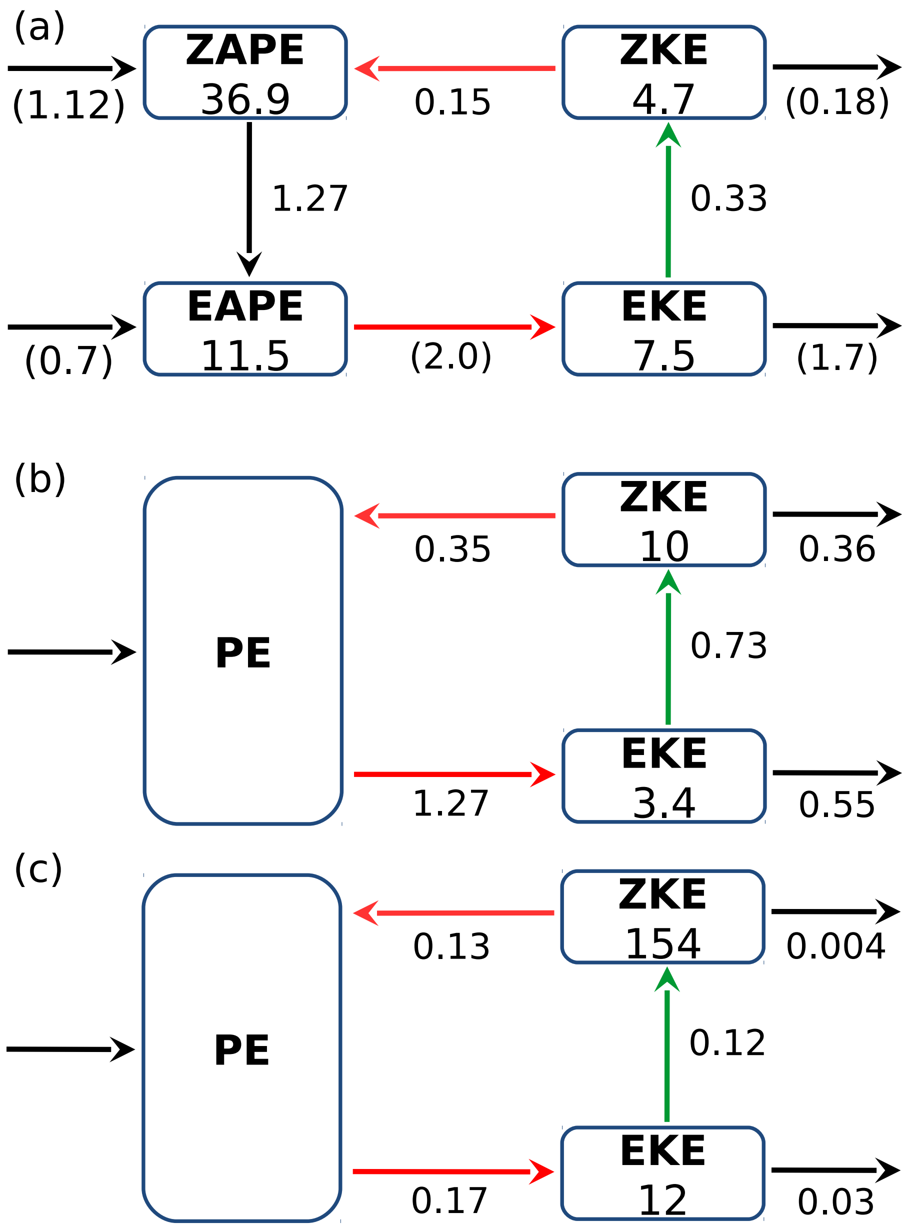

1003 FIG. 6. (a) The observed energy cycle for the global Earth's atmosphere. Energy amounts inside each box are
1004 given in 10^5 J m^{-2}, and rates of generation, conversion, and dissipation in W m^{-2}; not directly measured terms
1005 are shown in parentheses (adapted from Peixoto and Oort 1984). The energy cycle for Earth-like simulations
1006 with (b) the highest surface friction $\tau_f = 1$ day and (c) the lowest surface friction $\tau_f = 10^4$ days.

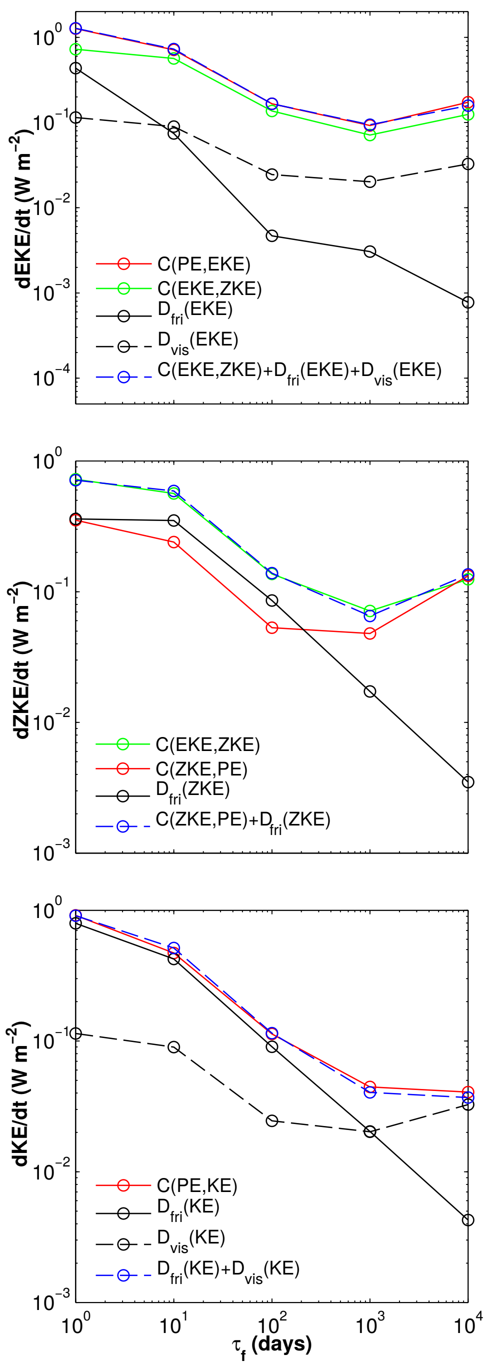

1007 FIG. 7. Rates of kinetic energy generation, conversion and dissipation in W m^{-2} for (top) eddy, (middle)
1008 zonal mean and (bottom) total flows for runs with different strength of surface friction.

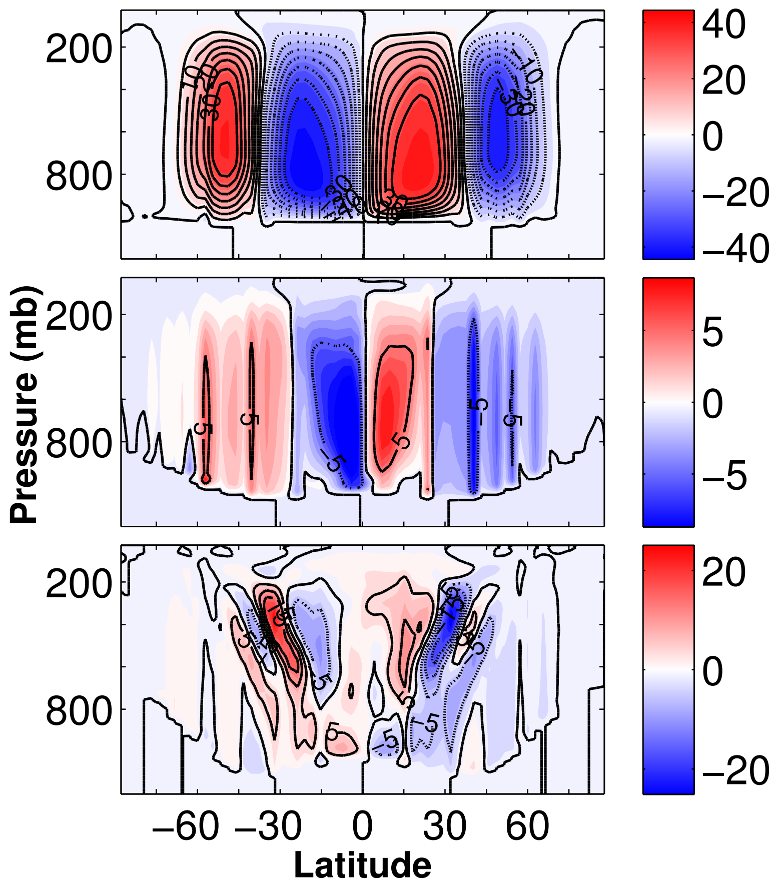

1009 FIG. 8. Time averaged zonal mean meridional circulation for Earth-like simulations with different strength
1010 of surface friction: τ_f =(top) 1, (middle) 10^2, and (bottom) 10^4 days. The unit is 10^9 kg s^{-1}, and the contour
1011 interval is 5×10^9 kg s^{-1}. Positive value denotes clockwise while negative value denotes counter-clockwise.

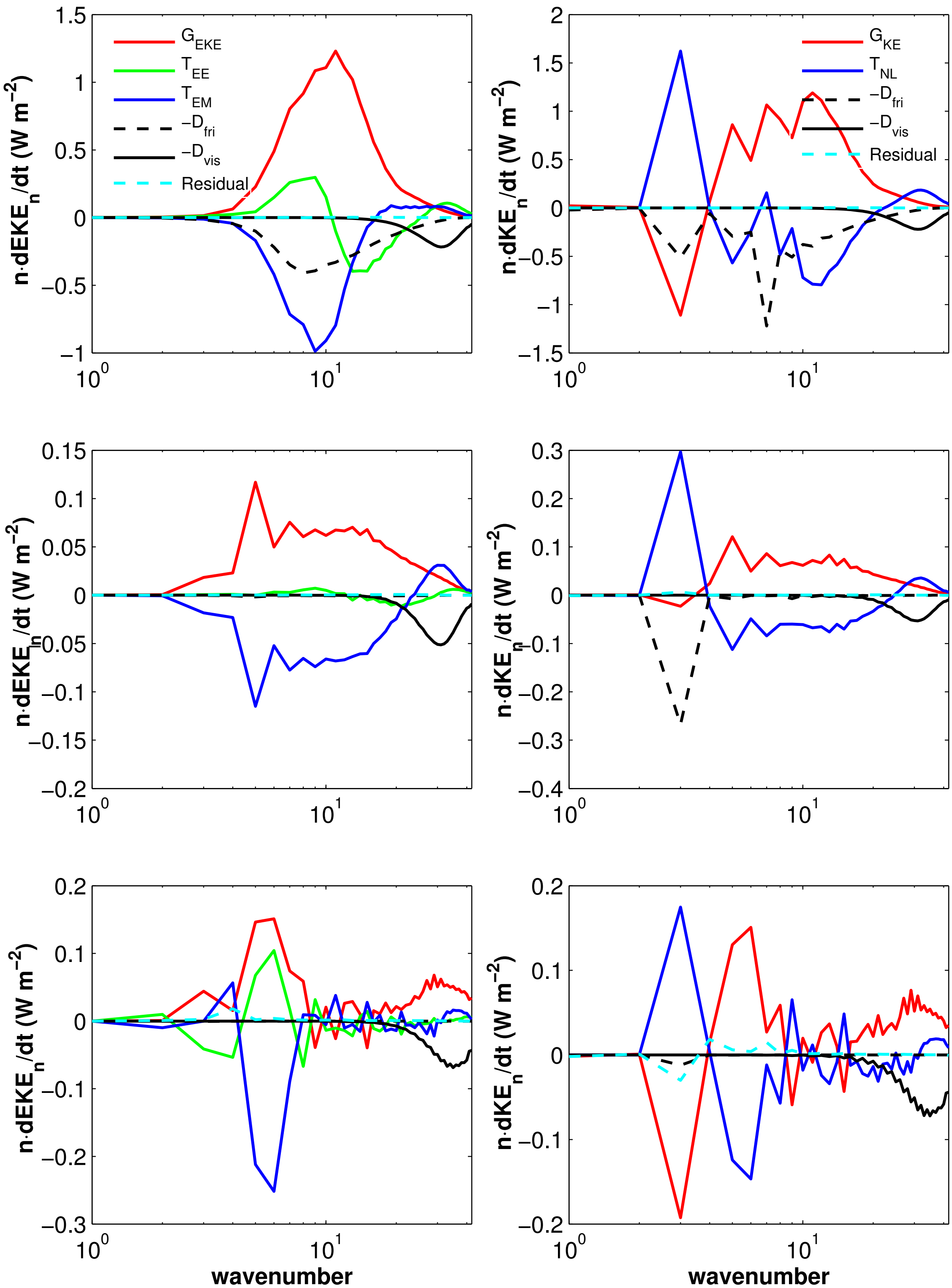

FIG. 9. (Left panel) Spectral EKE budget and (right panel) spectral KE budget for Earth-like simulations with various bottom friction: τ_f =(top) 1, (middle) 10^2, and (bottom) 10^4 days.

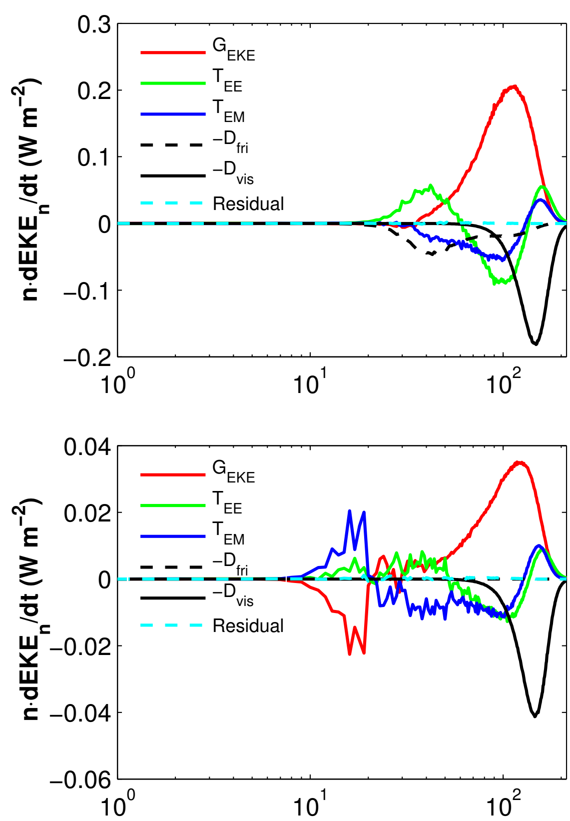

FIG. 10. Spectral EKE budget for Jupiter-like simulations with various bottom friction: $\tau_f =$ (top) 5 and (bottom) 5000 days.

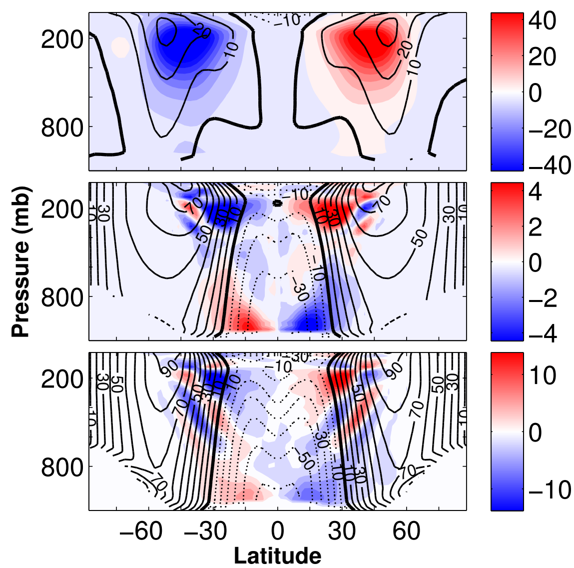

1016 FIG. 11. Eddy momentum flux together with zonal mean zonal wind for Earth-like simulations with various
1017 bottom friction: τ_f =(top) 1, (middle) 10^3, and (bottom) 10^4 days. The contour interval for zonal wind is 10
1018 m/s.

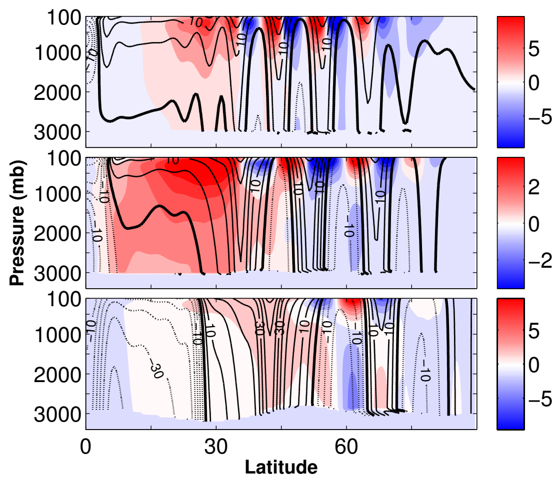

FIG. 12. Eddy momentum flux together with zonal mean zonal wind for Jupiter-like simulations with various bottom friction: (top) τ_f =5, (middle) 50 and (bottom) 5000 days. Only Northern hemisphere is shown as Southern hemisphere is nearly symmetric. The contour interval for zonal wind is 5 m/s.

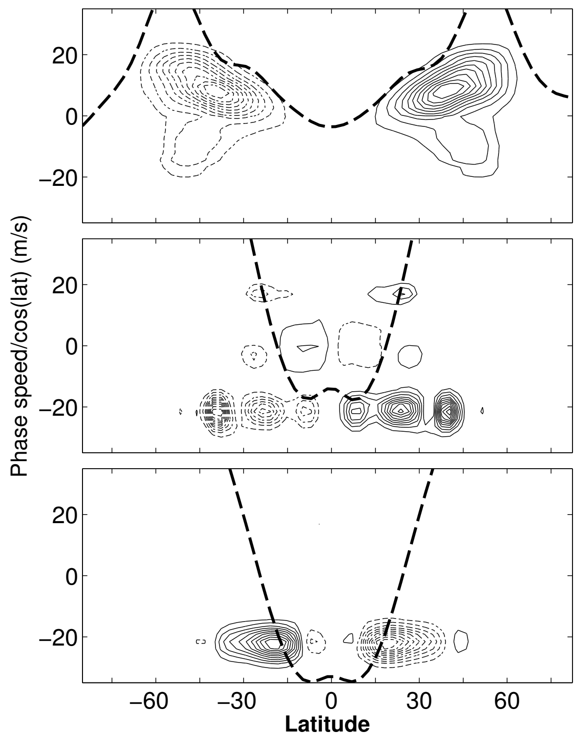

1022 FIG. 13. (Top) Eddy momentum flux phase speed cospectrum in the upper atmosphere ($\sigma = 0.316$) vs.
1023 latitude for Earth-like simulation with $\tau_f = 1$ day as a reference. The same spectra for Earth-like simulations
1024 with $\tau_f = 10^3$ days in the (middle) upper ($\sigma = 0.316$) and (bottom) lower ($\sigma = 0.816$) atmospheres. The
1025 thick black line shows temporal and zonal averaged zonal wind at the same level. The dashed contour denotes
1026 southward eddy momentum flux.

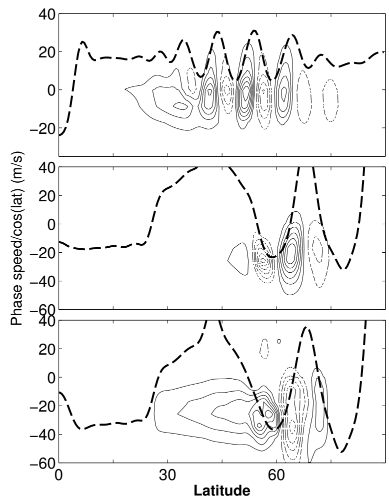

FIG. 14. Similar to Fig. 13 but for Jupiter-like simulations. (Top) Eddy momentum flux phase speed cospectrum in the upper atmosphere ($\sigma = 0.02$) vs. latitude for Jupiter-like simulation with $\tau_f = 5$ day as a reference. The same spectra for Jupiter-like simulations with $\tau_f = 5000$ days in the (middle) upper ($\sigma = 0.02$) and (bottom) lower ($\sigma = 0.84$) atmospheres. The thick black line shows temporal and zonal averaged zonal wind at the same level. The dashed contour denotes southward eddy momentum flux.

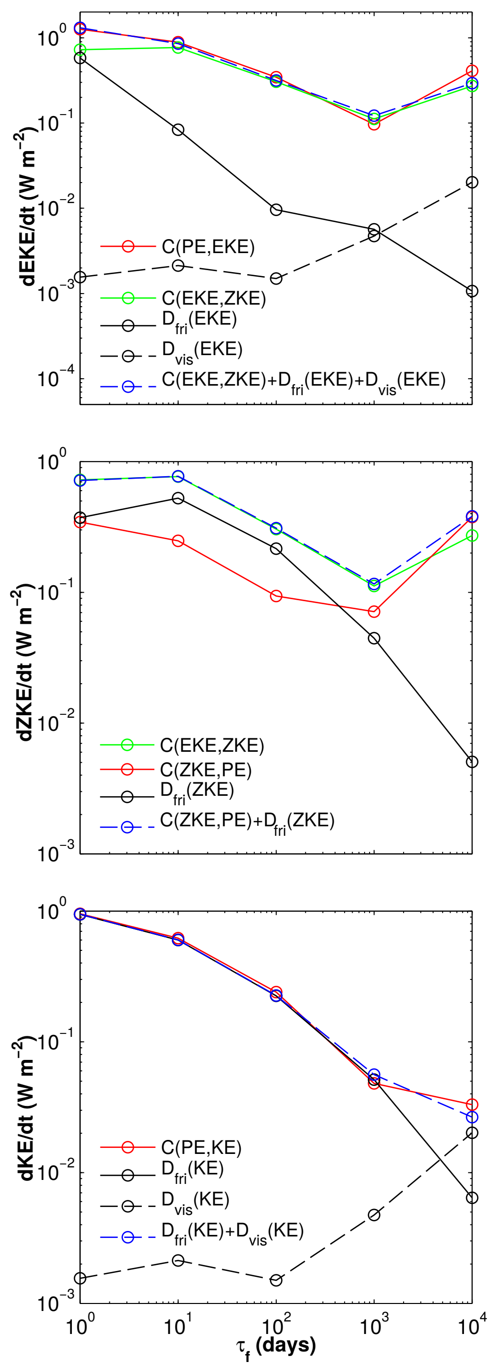

FIG. 15. Similar to Fig. 7 but for T127 simulations. Rates of kinetic energy generation, conversion, and dissipation in W m^{-2} for (top) eddy, (middle) zonal mean and (bottom) total flows for runs with different strength of surface friction.

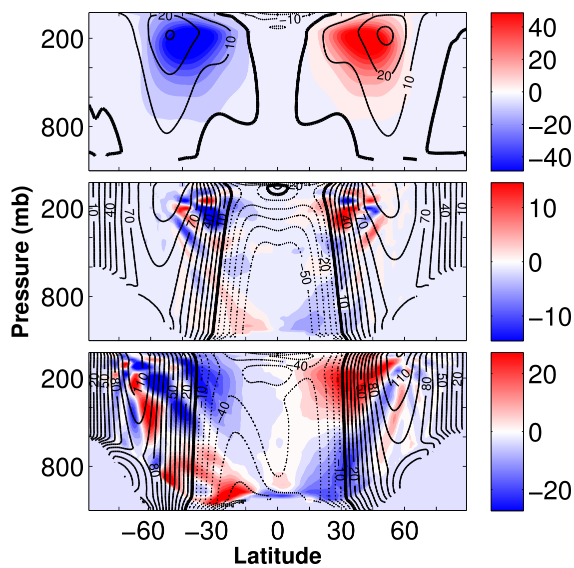

FIG. 16. Similar to Fig. 11 but for T127 simulations. Eddy momentum flux together with zonal mean zonal wind for Earth-like simulations with various bottom friction: τ_f =(top) 1, (middle) 10^3, and (bottom) 10^4 days. The contour interval for zonal wind is 10 m/s.

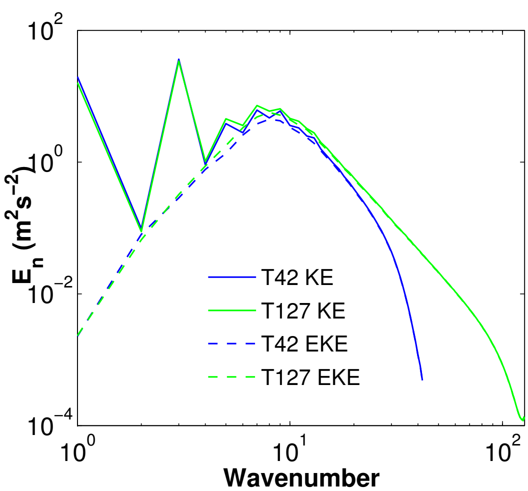

1038 FIG. 17. Total kinetic energy spectra (solid lines) and eddy kinetic energy spectra (dashed lines) from T42
1039 (blue lines) and T127 (green lines) Earth-like simulations with frictional time scale τ_f=1 day.

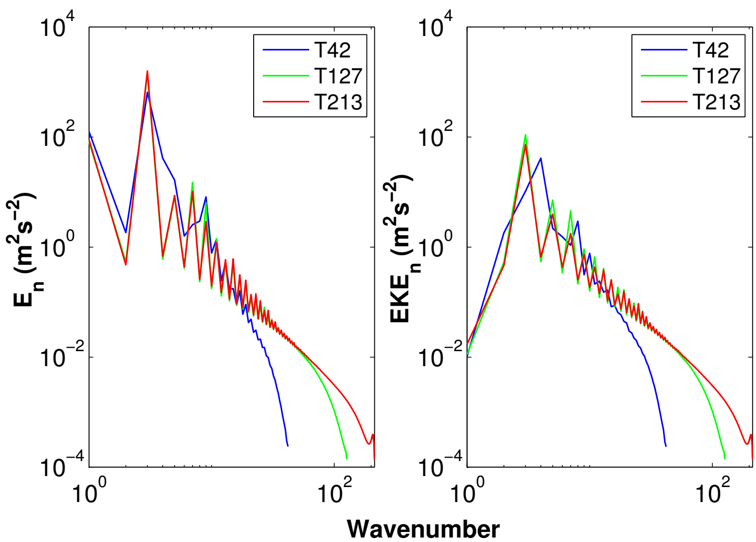

1040 FIG. 18. Total kinetic energy spectra (left) and eddy kinetic energy spectra (right) from T42 (blue lines), T127
1041 (green lines) and T213 (red lines) Earth-like simulations with frictional time scale τ_f=10^3 day.

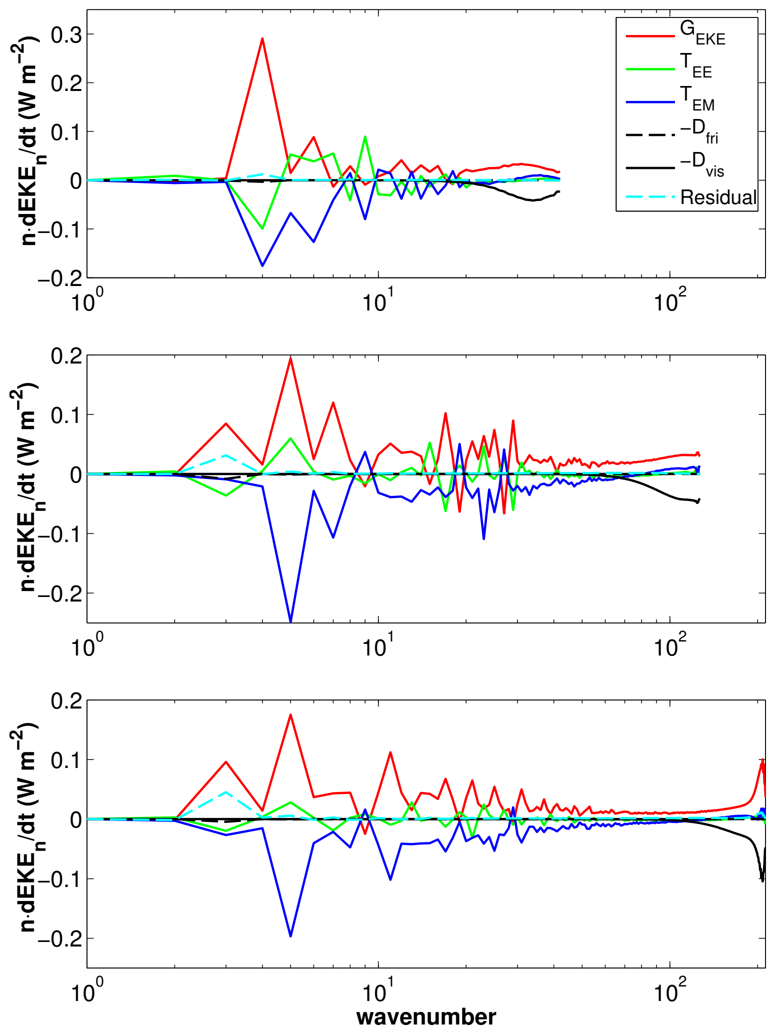

1042 FIG. 19. Spectral EKE budget for Earth-like simulations with bottom friction $\tau_f = 10^3$ days at various horizontal resolutions: (top) T42, (middle) T127 and (bottom) T213.

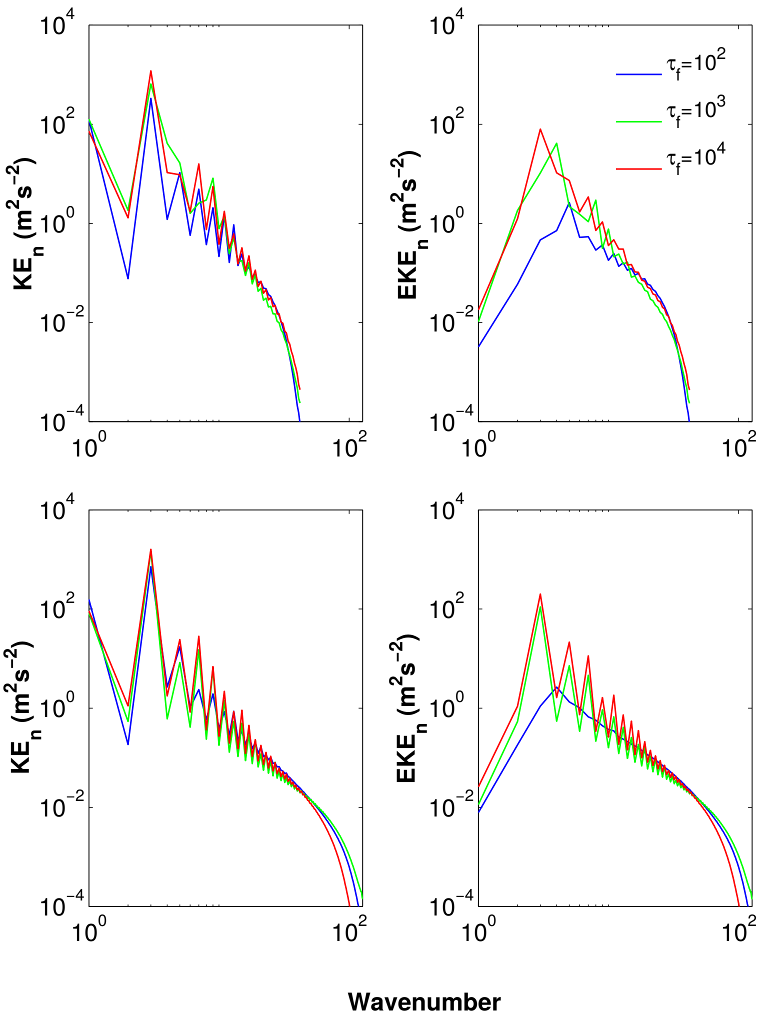

FIG. 20. Total kinetic energy spectra (left) and eddy kinetic energy spectra (right) from T42 (top), T127 (bottom) Earth-like simulations with various frictional time scales: τ_f=10^2, 10^3 and 10^4 day.

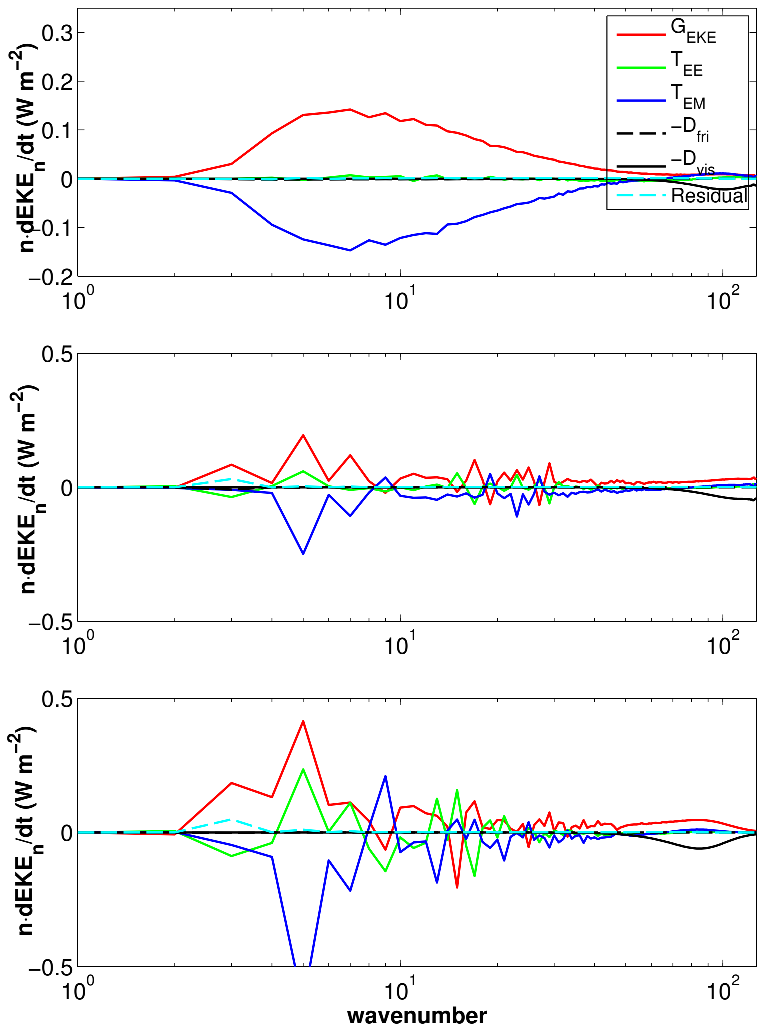

1046 FIG. 21. Spectral EKE budget for Earth-like simulations with horizonal resolution T127 and various bottom

1047 friction time scales: $\tau_f =$ (top) 10^2, (middle) 10^3 and (bottom) 10^4 days.

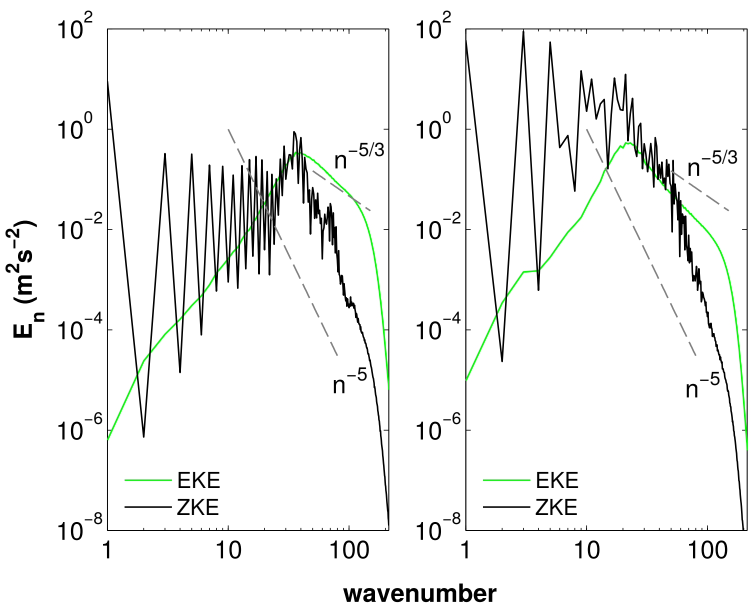

FIG. 22. Eddy kinetic energy spectrum (solid green line) and zonal kinetic energy spectrum (solid black line) for Jupiter-like simulations with frictional time scale τ_f =(left) 5 days and (right) 5000 days. The dashed gray lines show spectrum slope of -5 and -5/3.

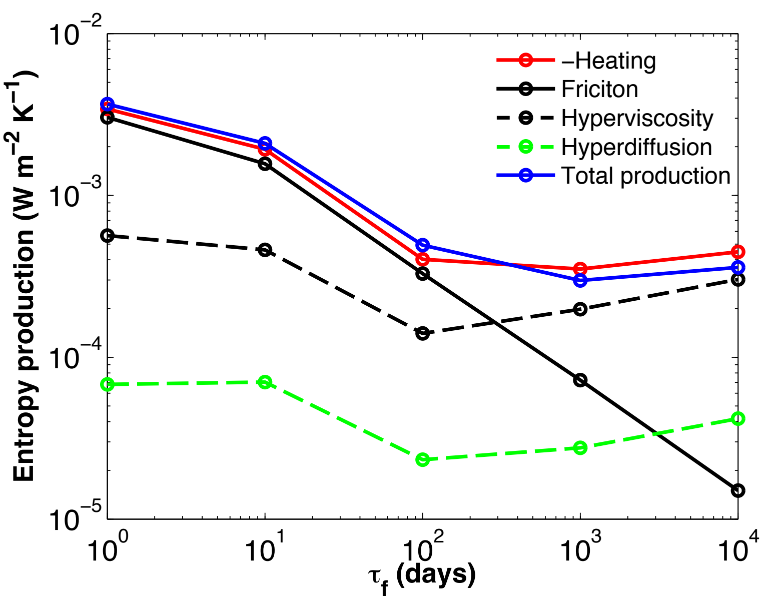

FIG. 23. Entropy budget for the Earth-like simulations with various bottom friction. The entropy sink by radiative forcing is shown by its absolute value for plotting in logarithm coordinate.